Commissioning of a PMT test facility for JUNO

Inbetriebnahme eines PMT-Teststandes für JUNO

by

Felix Sorgenfrei

born:

19.10.1994

Bachelorarbeit im Studiengang Physik
Universität Hamburg

2017

1.Reviewer: Prof. Dr. Caren Hagner

2.Reviewer: Dr. Björn Wonsak

Abstract

JUNO is a 20 kt liquid scintillator anti neutrino detector equipped with 18000 20-inch photomultiplier tubes (PMTs) for light detection, that is currently being build in China to determine the neutrino mass hierarchy. The mass hierarchy has a fundamental role in astronomy and cosmology. It can also be an important factor to measure the CP-violating phase. Furthermore it can give a clue for a better understanding whether the neutrino is a Dirac or a Majorana particle.For this, an unprecedented energy resolution of 3% at 1 MeV is needed. To reach this resolution all PMTs need to be shielded against the earth magnetic field as it decreases the performance of them. To reach the energy resolution the earth magnetic field needs to be reduced to 10%. Furthermore all the PMTs need to be tested and calibrated thoroughly. For the purpose of creating the same conditions in the testing facility and the experiment, the test facilities for the 20-inch PMTs have to be shielded against the magnetic field. In course of this thesis the magnetic field inside these facilities is measured. This shows that the magnetic field meets the requirements at most the measured points. Also a quick way to strengthen the shielding after transportation damage will be presented. Furthermore methods for the characterization of PMTs are introduced. Because problems with the tubes used for an homogeneous light distribution in the testing facility in China arose, every part of the tubes is tested. These parts are cardboard, Tyvek and glue, which connects the other two. A light emission effect of the glue is discovered and an alternative way of construction by using stainless steel staples instead is presented and tested.

Zusammenfassung

Juno ist ein 20 kt flüssig Scintillator Anti Neutrino Detektor, der in China gebaut wird, um die Neutrino Massenhierachy zu bestimmen. Die Massen Hierachie hat eine fundamentale Rolle für Astronomie und Kosmologie. Auch kann sie ein wichtiger Faktor zur Bestimmung der CP-verletzenden Phase sein. Desweiteren kann sie einen Hinweis liefern, um besser zu verstehen ob das Neutrino ein Dirac oder Majorana Teilchen ist. Dieser Detektor ist mit 18000 Photomultiplier Tubes (PMTs) ausgestatet, um das Licht des Scintillators zu messen. Dafür wird eine bisher unerreichte Energieauflösung von 3% bei 1 MeV gebraucht. Um diese Auflösung zu erreichen müssen alle PMTs gegen das Erdmagnetfeld geschützt werden, da es die Performance dieser einschränkt. Desweiteren müssen alle PMTs gründlich getested und kalibriert werden. Um die selben Bedingungen im Teststand wie im späteren Experiment zu kreieren, müssen die Teststände für die 20-inch PMTs gegen das Magnetfeld geschützt sein. Zum Erreichen der Energieauflösung soll das Magnetfeld auf 10% reduziert werden. Im Laufe dieser Arbeit wurde das Magnetfeld in den Testständen gemessen. Dieses erfüllt die Vorgaben an den meisten Stellen. Zusätzlich wird eine Methode Schäden an der Abschirmung, die beim Transport entstehen, schnell auszubessern vorgesstellt. Desweiteren werden Methoden zur Charakterisierung von PMTs vorgestellt. Weil ein Problem mit den Röhren, die für eine gleichmäßige Lichtverteilung sorgen sollen, im Teststand in China aufgetaucht ist, werden alle Bestandteile getestet. Die Bestandteile der Röhre sind Pappe, Tyvek und Klebe, welche beide verbinded. Eine Emission von Licht der Klebe wird gefunden und ein alternativer Weg zur Konstruktion durch die Nutzung von Edelstahl Tackern wird vorgetellt und getested.

Contents

1 Introduction

The Standard Model was proven to be incomplete over the last decades. One of the most prominent examples for this is the flavour oscillation of neutrinos. The flavour oscillation requires the neutrinos to be massive leptons with mixing mass eigenstates. The mass hierarchy, which is the ordering of these mass eigenstates, was not determined as of now.

The determination of the mass hierarchy is the main focus of the Jiangmen Underground Neutrino Observatory (JUNO). JUNO is a liquid scintillator anti neutrino detector (LAND). The detector is placed inside a water tank with veto photomultiplier tubes (PMTs). The central detector holds 20 kt of linear Alkyl-Benzyne (LAB) scintillator material inside an acrylic ball. The ball is encased by a stainless steel latticed shell. This shell will hold up to 18000 20-inch PMTs and 25000 smaller 3-inch PMTs. The anti neutrinos for the measurements will be provided by two nuclear power plants close to the experimental site. To determine the mass hierarchy the detector is required to have an unprecedented sensitivity of at least 3% at 1 MeV. For this the PMTs have to be tested thoroughly.

The 20-inch PMTs will be tested and calibrated individually inside four shipping containers, which were developed by the University of Hamburg and the Eberhard-Karls-University Tübingen.

This thesis focuses on tests on smaller 2-inch PMTs inside a small laboratory test facility. These tests are dark current measurements, the classification of the single photon peak and the construction of an coincidence circuit. Furthermore the materials of the tubes used for a homogeneous light distribution in the test facility will be tested, as the PMTs showed an increased dark current rate, when placed in front of them. This provides an insight in the testing mechanisms, that will be used for the 20-inch PMTs in China.

Because external magnetic fields have a negative effect on the performance of the PMT, the JUNO central detector is shielded against the earth magnetic field with two coils. In order to have the same performance during the calibration and the detector measurements the shipping containers need to be shielded against the earth magnetic field as well. For this the test stand is equipped with a passive soft iron shielding. The shielding will be tested and a way to improve damaged shielding will be discussed.

In chapter 2.1 covers the basic information about neutrino physics leading to the flavour oscillation and the mass hierarchy, which are relevant for the JUNO experiment. The chapter 2.2 outlines general information about the JUNO-experiment. The working principle of PMTs and various influences on the measurements will be provided in chapter 2.3. In chapter 3.2 the magnetic field measurements will be discussed. Chapter 3.3.2 the dark current spectrum of the 2-inch PMT in the laboratory will be analyzed and characterized. For this the the the voltage region, where single photon events are expected, was determined. The materials of the tubes were tested in chapter 20. Chapter 3.3.4 deals with the construction of a coincidence circuit to reduce the background noise.

2 Theory

This chapter gives the basic information to understand what the JUNO-experiment is about. In the first chapter 2.1 the theory behind the neutrinos leading to the mass hierarchy will be discussed, whose unraveling is one of the main goals of the project. After that the JUNO-experiment will be outlined further in chapter 2.2. At last the main measurement tool used in this experiment, the photomultiplier tubes, will be commented on in chapter 2.3.

2.1 Particle and Neutrino Physics

Particle physics deals with all fundamental particles and their interactions. Inside particle physics the neutrino holds a special position. Originally introduced as massless particles to solve the conservation of energy and momentum for the β-decay, they now show more and more interesting effects limited to these particles. In the following chapter particle physics will be introduced by explaining the Standard Model (2.1.1). After that neutrinos in general with special care for neutrino flavour oscillation will be explained (2.1.2) and thereafter the mass hierarchy (2.1.3).

2.1.1 Standard Model

Although not complete, the Standard Model of particle physics summarizes most knowledge about particles and their interactions we have. For the description it uses quantum field theory (QFT), which is a combination of quantum mechanics and classical field theory. Based on the local gauge group

$$SU(3)_c \times SU(2)_c \times U(1)_y, \tag{1}$$

it describes the strong and the electroweak interaction. The electroweak interaction is a combination of the electric and the weak interaction. So the gauge groups only explain three of the four fundamental interactions as gravitation is not included in the Standard Model, because there is no theory that can combine general relativity and quantum field theory. The graviton, the gauge boson, which is the postulated gauge boson for gravity, has not been found yet. This boson should have spin 2, for an attractive interaction with a charge of the same sign. The electroweak interaction unifies the electric and the weak interaction and is described by the $SU(2)_c \times U(1)_y$ group. The strong interaction follows

from the $SU(3)_c$ group. The interactions are described with the exchange of gauge bosons. Bosons are particles with integral spin. The particles that exchange these gauge boson are fermions. All elementary fermions have spin $\frac{1}{2}$ and every other fermion is a combination of an uneven number of elementary fermions. The Standard Model is often illustrated by a table containing every elementary particle as seen in figure 1. It gives a brief summary of spin, mass, charge and the characterizing group of the particle. All particles have an antiparticle with the same mass but all quantum numbers (charge, lepton number etc.) change sign. Particles can also be their own antiparticle, these particles are called Majorana particles. But for that all the additive quantum numbers need to vanish. For the elementary particles this is only the case for the photon and the Z^0-boson, at least as far as the Standard Model is concerned. Particles that are different from their antiparticle are called Dirac particles.

The gauge boson of the strong interaction is the gluon. It is massless and has colour charge, which is a combination of the three colours, red r, blue b and green g and their anticolours (antired $\bar{r}$, antiblue $\bar{b}$ and antigreen $\bar{g}$). The number of possible anticolour and colour combinations can be derived via group theory. It is $3 \otimes 3 = 8 \oplus 1$. The direct product of a colour triplet and an anticolour triplet forms a direct sum of an octet and a singlet. But the singlet state cannot be observed. So there are eight different states the gluon can be in. The only particles that interact with the gluons are the quarks and other gluons as they are the only particles that carry a colour charge. The quarks are divided in two families and three generations. Each generation is split in up- and down-type quarks, named after their first generation members. Up-type quarks consist of up, charm and top (u,c,t) and have an electric charge of $\frac{2}{3}e$. This e is the elementary charge with $e = 1.602 * 10^{-19}$ C. The down-type quarks consist of down, strange and bottom quark (d,s,b). They have an electric charge of $-\frac{1}{3}e$. These quarks have a colour and their antiparticles have an anticolour. Quarks can only exist alone for very short times ($t_{had} = 3 * 10^{-24}$ s)[28], they need to be in bound states. This phenomenon is referred to as quark confinement. For a bound state the colour charge needs to add up to white. This happens by combining one colour with its anticolour in mesons or by combining all three colours or anticolours in baryons. So a meson consists of a quark and an antiquark and a baryon is made out of three quarks or antiquarks. Of course bond states are also possible for a higher number of quarks, like the already observed penta quarks.

The gauge boson of the electric interaction is the photon, which is without mass and electric charge. It interacts with all particles that have an electric charge, so all the quarks and the charged leptons. Because it does not have mass and there is no confinement involving the electric charge, the photon has an unlimited interaction length. Leptons have the quantum number of lepton number, which is conserved under all interactions within the realms of the Standard Model. Leptons are split into charged leptons (electron e, muon μ and tau τ), which have an electric charge of -1, and the neutrinos named after their charged leptonic generation member (ν_e, ν_μ, ν_τ). Neutrinos have no electric charge and are massless within the Standard Model. This is why they are only affected by the weak interaction. The gauge bosons of the weak interaction are the Z and the W boson. The Z boson is responsible for neutral currents and the main reason the weak and the electric interaction were unified. The $W^\pm$ boson has a charge of ± 1. Because of their relatively high mass ($m_Z = (91.1876 \pm 0.0021)\,\text{GeV}[3]$, $m_{W^\pm} = (80.385 \pm 0.015)\,\text{GeV}[3]$), the weak interaction has a short range.

The last elementary particle inside the Standard Model is the higgs boson. It has a mass of $126\,\text{GeV}$ and it interacts with all massive elementary particles. It provides the fundamental particles with mass via electroweak symmetry breaking [46].
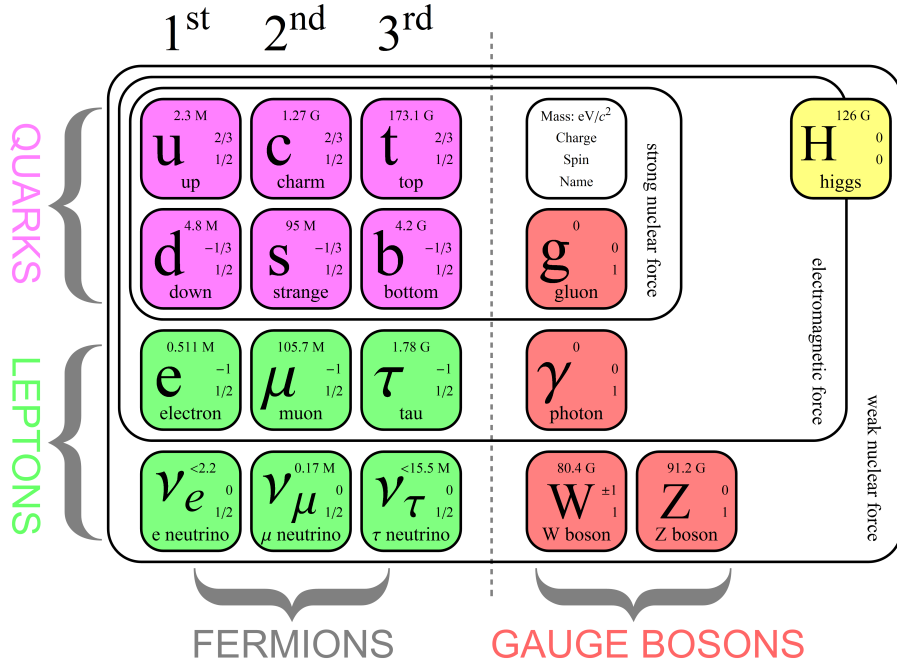
Figure 1: These are all the elementary particles described inside the Standard Model. The fermions are on the left the bosons on the right. The fermions are then split into three different columns from left to right representing the different generations. The top two rows show the quarks in pink, the lower the leptons in green. Both of them are split horizontally into their individual families. The bosons all encircle the fermions they interact with. The top number represents the mass of the particle in eV, the one in the middle the charge in e (elementary charge) and the lowest represents the spin[2].

2.1.2 Neutrino Physics

Neutrinos were first introduced by Pauli to explain the conservation of energy and linear momentum for the β-decay. The anti electron neutrino was later introduced after the observation of the inverse β-decay

$$\bar{\nu}_e + p = n + e^+ \tag{2}$$

Here a proton p and an anti electron neutrino $\bar{\nu}_e$ collide and form a positron e^+ and a neutron. The helicity is defined as the projection of a particle's spin on its momentum direction and has the eigenvalues $\pm\frac{1}{2}$ for these fermions. For massless particles the helicity is equal to the quantuum mechanical component of chirality. This chirality has two eigenstates, right handed or left handed. The $W^\pm$ interacts only with left handed fermions and right handed anti fermions. The discovery that neutrino are left-handed and anti neutrinos right-handed was made by Wu [4] and Goldhaber [5]. Because neutrinos are massless within the Standard Model, they have a helicity of $-\frac{1}{2}$ are left handed and antineutrinos

9

with a helicity of $\frac{1}{2}$ are right handed. This results in a violation of parity, which is the symmetry property of a system towards spatial inversion. A parity inversion $\mathcal{P}$ changes the sign of the spacial coordinates,x,y,z:

$$\mathcal{P} : \left(x, \quad y, \quad z\right) \rightarrow \left(-x, \quad -y, \quad -z\right). \tag{3}$$

This would transform a right-handed coordinate system into a left-handed one and the other way around. If this is applied on a process containing a neutrino, the chirality of the neutrino would change, which it cannot do resulting in a not conserved or violated parity. By also changing all charges with a $\mathcal{C}$ transformation and so transforming a particle into its antiparticle, this problem is avoided. The combination of $\mathcal{C}$ and $\mathcal{P}$ transformations is called $\mathcal{CP}$ transformation. In 1964 James W. Corwin and Val Fitch proved that the $\mathcal{CP}$ symmetry can be broken using the decay of kaons [36]. Analog to the parity violation this is referred to as CP violation.

The idea of neutrino flavor oscillation was first introduced by *B. Pontecorvo* in 1967 [30], after the discovery of ν_μ at *Brookhaven lab* in 1962 [31]. With his work he predicted the solar neutrino problem [30]. In the early 1970s Davis observed a deficit of ν_e from the expected in the flux of the solar spectrum. The results of this *Homestake Experiment* was validated by similar experiments as they all came to the same conclusion. The first clear results of a mixed neutrino spectrum within the sun's flux was given by the *Sudbury Neutrino Observatory* (SNO) in 2001[34]. These results could be explained with *B.Pontecorvos* flavour mixing after the expansion for the third flavour, as the ν_τ had been found in the mean time. But this requires the neutrinos to have mass, which will be explained later. As lepton flavour and number conservation are not based on a fundamental symmetry, there is no reason to believe the flavour must be constant in a reaction. But this requires the eigenstates for the mass and the flavour to be different, because for the conservation of energy and linear momentum it is necessary for the neutrino to keep its mass, while it changes the flavour. So the weak eigenstates are

$$|\nu_\alpha\rangle, \alpha = e, \mu, \tau \tag{4}$$

and the mass eigenstates are

$$|\nu_j\rangle, j = 1, 2, 3. \tag{5}$$

But as they both form a three dimensional orthogonal base for the same three dimensional room, an eigenstate can always be written as a linear combination of the three eigenstates from the other aspect [6]:

$$|\nu_\alpha\rangle = \sum_j U_{\alpha j}|\nu_j\rangle \qquad \text{and} \qquad |\nu_j\rangle = \sum_\alpha U_{\alpha j}^*|\nu_\alpha\rangle, \qquad (6)$$

where $U_{\alpha j}$ is the entry of the unitary Pontecorvo-Maki-Nakagawa-Sakata (PMNS)matrix U, and $U_{\alpha j}^*$ their complex conjugate. It contains three mixing angles and one phase for three flavours. For antineutrino oscillation the same formulas apply, but $U_{\alpha j}$ and $U_{\alpha j}^*$ are always swapped:

$$U = \begin{pmatrix} c_{12}c_{13} & s_{12}c_{13} & s_{13}e^{-i\delta} \\ -s_{12}c_{23} - c_{12}s_{13}s_{23}e^{i\delta} & c_{12}c_{23} - s_{12}s_{13}s_{23}e^{i\delta} & c_{13}s_{23} \\ s_{12}s_{23} - c_{12}c_{23}s_{13}e^{i\delta} & -c_{12}s_{23} - s_{12}s_{13}c_{23}e^{i\delta} & c_{13}c_{23} \end{pmatrix} P_\nu \qquad (7)$$

c_{ij} stands for $cos(\theta_{ij})$, while s_{ij} stands for $sin(\theta_{ij})$ where θ_{ij} is the mixing angle between state i and state j with $i \neq j$ and $i, j \in 1,2,3$. δ is the CP violating phase. P_ν represents the Majorana phase, which is indifferent for Dirac neutrinos. Because P_ν is a phase and so $1 = |P_\nu|^2$, it is not relevant for the oscillation. This can be seen later as all $U_{\alpha j}$ are always paired with their complex conjugate, so P_ν is always paired with its complex conjugate.

The mass eigenstates need to be stationary states for energy and momentum conservation with an observed time dependency of [6]:

$$|\nu_i(x,t)\rangle = e^{-iE_j t}|\nu_i(x)\rangle, \qquad (8)$$

where E_j is the energy of the respective mass eigenstate and t is the time. The local dependence shown at time $t = 0$ and source located at $x = 0$ and an assumed momentum p is [6]:

$$|\nu_i(x,0)\rangle = e^{ipx}|\nu_i\rangle \qquad (9)$$

Here x is the distance to its starting point. Neutrinos are produced and detected in flavour eigenstates, therefore it is more beneficial to describe the flavour eigenstates. Using

equation$(6), (8)$and(9) it follows [6]

$$|\nu_\alpha(x,t)\rangle = \sum_j U_{\alpha j} e^{-iE_j t}|\nu_j\rangle = \sum_{\beta,j} U_{\alpha j} U_{\beta j}^* e^{ipx} e^{-iE_j t}|\nu_\beta\rangle. \tag{10}$$

As neutrinos still need to be relativistic ($m \ll p$ and $cp \approx E$), E_j can be expressed as

$$E_j = \sqrt{m_j^2 + p_j^2} \simeq p_j + \frac{m_j^2}{2p_j} \simeq E + \frac{m_j^2}{2E}. \tag{11}$$

Using (9) and (10) the probability for a neutrino to change flavour can be expressed as [6]

$$P(\alpha \to \beta)(\frac{L}{E}) = |\langle\nu_\beta|\nu_\alpha(x,t)\rangle|^2 = \left|\sum_j U_{\alpha j} U_{\beta j}^*\right|^2 + 2Re\left[\sum_{k>j} U_{\alpha j} U_{\alpha k}^* U_{\beta j}^* U_{\beta k} \exp\left(-i\frac{\Delta m_{jk}^2}{2}\frac{L}{E}\right)\right],$$
$$\tag{12}$$

with $L = x \approx ct$ being the length the neutrino travels from its source to the detector. $\Delta m_{jk}^2 = m_j^2 - m_k^2$ is the difference of the quadratic masses from the different eigenstates. This can be simplified if $U_{\alpha j}$ are assumed as real (CP-invariance), to [6]:

$$P(\alpha \to \beta)(\frac{L}{E}) = \delta_{\alpha\beta} - 4\sum_{k>j} U_{\alpha j} U_{\alpha k} U_{\beta j} U_{\beta k}\sin^2\left(\frac{\Delta m_{jk}^2 L}{4E}\right), \tag{13}$$

this shows that the frequency of the oscillation depends on Δm_{jk}^2 as well as $\frac{L}{E}$. The dependency on Δm_{jk}^2 shows that at least two of the mass eigenstates need to be different from zero. Furthermore it shows that the eigenvalues of the different mass eigenstates need to be different for flavour oscillation to occur.

2.1.3 Mass Hierarchy

Combining equation (7) and (13), we get 6 defining constant parameters for the neutrino oscillation of Dirac neutrinos, namely the CP-violating phase δ, the two differences of the quadratic masses Δm_{12}^2 and Δm_{13}^2 and the three mixing angles θ_{12}, θ_{13} and θ_{23}. Only two Δm_{ij}^2 are independent of each other, because $\Delta m_{23}^2 = \Delta m_{13}^2 - \Delta m_{12}^2$. So Δm_{12}^2 is not an defining parameter. Most of them are already measured by previous experiments. Their values are shown in table 1. This leaves only δ and Δm_{13}^2 unknown, but not completely as the absolute value of Δm_{13}^2 has been identified. This leaves two ways for the masses to be

Table 1: Values of the different neutrino oscillation parameters and their σ areas in dependency of the assumed mass hierarchy. This table is taken from [14] and it is based on data from [15].

Parameter	Best fit	1σ range	2σ range	3σ range
Normal mass hierarchy				
$\Delta m_{21}^2 * 10^5 \text{eV}^2$	7.54	7.32-7.80	7.15-8.00	6.99-8.18
$\Delta m_{31}^2 * 10^3 \text{eV}^2$	2.47	2.41-2.53	2.34-2.59	2.26-2.65
$\sin^2(\theta_{12}) * 10$	3.08	2.91-3.25	2.75-3.42	2.59-3.59
$\sin^2(\theta_{13}) * 100$	2.34	2.15-2.54	1.95-2.74	1.76-2.95
$\sin^2(\theta_{23}) * 10$	4.37	4.14-4.70	3.93-5.52	3.74-6.26
$\delta/180°$	1.39	1.12-1.17	$0.00 - 0.16 \oplus 0.86 - 2.00$	0.00-2.00
Inverted mass hierarchy				
$\Delta m_{21}^2 * 10^5 \text{eV}^2$	7.54	7.32-7.80	7.15-8.00	6.99-8.18
$\Delta m_{31}^2 * 10^3 \text{eV}^2$	2.42	2.36-2.48	2.29-2.54	2.22-2.60
$\sin^2(\theta_{12}) * 10$	3.08	2.91-3.25	2.75-3.42	2.59-3.59
$\sin^2(\theta_{13}) * 100$	2.40	2.18-2.59	1.98-2.79	1.78-2.98
$\sin^2(\theta_{23}) * 10$	4.55	4.24-5.94	4.00-6.20	3.80-6.41
$\delta/180°$	1.31	0.98-1.60	$0.00 - 0.02 \oplus 0.70 - 2.00$	0.00-2.00

ordered:

$$m_1^2 < m_2^2 < m_3^2 \qquad \text{and} \qquad m_3^2 < m_1^2 < m_2^2, \qquad (14)$$

as seen in figure 2 with the known mass difference values and the neutrino flavour mixing of the mass eigenstates already integrated.

This is referred to as the mass hierarchy (MH), the left option is called normal hierarchy (NH) and the one on the right is called inverted hierarchy (IH).

Δm_{13}^2 can be measured by looking at the survival rate of $\bar{\nu}_e$, which is given by [6]

$$
\begin{aligned}
P(\bar{\nu}_e \to \bar{\nu}_e) =& 1 - \sin^2(2\theta_{12})c_{13}^4\sin^2\left(\frac{\Delta m_{12}^2 L}{4E}\right) \\
& - \sin^2(2\theta_{13})\left[c_{12}^2\sin^2\left(\frac{\Delta m_{13}^2 L}{4E}\right) + s_{12}^2\sin^2\left(\frac{\Delta m_{23}^2 L}{4E}\right)\right].
\end{aligned}
\qquad (15)
$$

The first two terms are given by the dominant 12-Oscillation. Because of the symmetry of $\sin^2$ the sign of Δm_{13}^2 can not be easily determined. The difference shows itself by the oscillation frequency of $\sin^2(\frac{\Delta m_{23}^2 L}{4E})$, because $|m_{23}^2|$ in the inverted hierarchy is bigger than in the normal hierarchy by $2m_{21}^2$. Another way to show the difference between the mass hierarchies is by using the total mass difference from the highest Δm^2 to the lowest. So
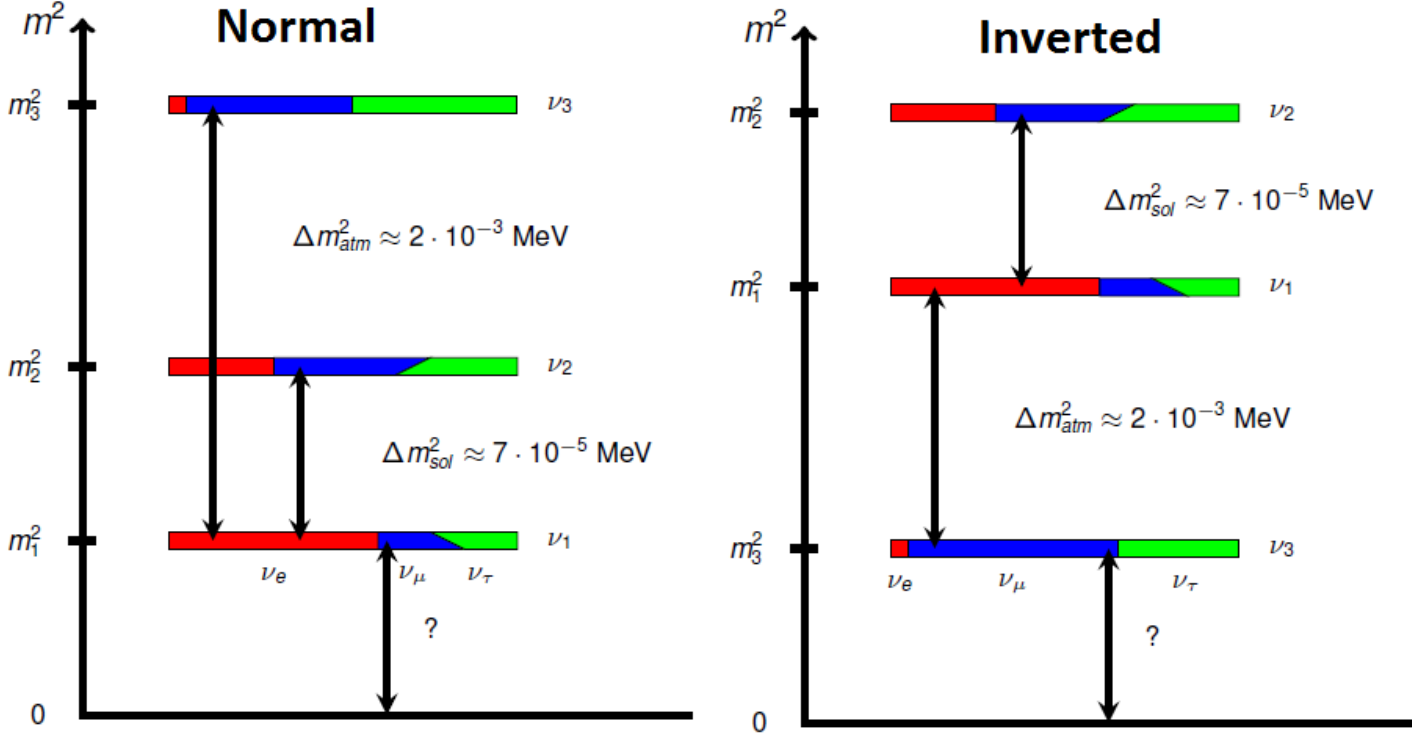
Figure 2: This illustrates the hierarchy of the different mass eigenstates and their share of lepton flavour eigenstates is expressed through the colours. This picture is an adapted version of [8]

$\Delta m_{com}^2 = \Delta m_{31}^2$ for NH and $\Delta m_{com}^2 = \Delta m_{23}^2$ for IH. Also $\delta m_{sol}^2 = \Delta m_{12}^2$ will be used [16].

$$
\begin{aligned}
P_{\mathrm{NH}}(\bar{\nu}_e \to \bar{\nu}_e) =& 1 - \frac{1}{2}\sin^2(2\theta_{13})\left[1 - \cos\left(\frac{\Delta m_{com}^2 L}{2E}\right)\right] \\
& - \frac{1}{2}c_{13}^4\sin^2(2\theta_{12})\left[1 - \cos\left(\frac{\delta m_{sol}^2 L}{2E}\right)\right] \\
& + \frac{1}{2}\sin^2(2\theta_{13})s_{12}^2\left[\cos\left(\frac{L}{2E}(\Delta m_{com}^2 - \delta m_{sol}^2)\right) - \cos\left(\frac{\Delta m_{com}^2 L}{2E}\right)\right]
\end{aligned}
\tag{16}
$$

$$
\begin{aligned}
P_{\mathrm{IH}}(\bar{\nu}_e \to \bar{\nu}_e) =& 1 - \frac{1}{2}\sin^2(2\theta_{13})\left[1 - \cos\left(\frac{\Delta m_{com}^2 L}{2E}\right)\right] \\
& - \frac{1}{2}c_{13}^4\sin^2(2\theta_{12})\left[1 - \cos\left(\frac{\delta m_{sol}^2 L}{2E}\right)\right] \\
& + \frac{1}{2}\sin^2(2\theta_{13})c_{12}^2\left[\cos\left(\frac{L}{2E}(\Delta m_{com}^2 - \delta m_{sol}^2)\right) - \cos\left(\frac{\Delta m_{com}^2 L}{2E}\right)\right]
\end{aligned}
\tag{17}
$$

The only difference between the two equations is that in the last term the $s^2(\theta_{12})$ for the NH changes to $c^2(\theta_{12})$ for the IH. Also the values of Δm^2_{com} differ by m^2_{sol} depending on the mass hierarchies. This also results in a faster suboscillation frequency for the Inverted mass hierarchy. The influences of these suboscillation in comparison to each other and the dominant 12 oscillation from the first two terms of equation (15) are illustrated in figure 3. It shows the neutrino oscillation based on the parameters for the different neutrino oscillations. The dotted line shows the expected curve for a non oscillating particle, the black the normal oscillation shown in the first two terms of equation (15). The red now shows the oscillation for the inverted mass hierarchy after equation(17) and the blue the normal hierarchy(16). Because the frequencies differ slightly, the mass hierarchy can best be determined around $10.5 \frac{km}{MeV}$, where the amplitudes are furthest apart as seen in figure 3. The measurements to tell the two apart need an energy resolution of at least 3% per MeV. Another way to determine the mass hierarchy is by using the altered flavour composition of atmospheric neutrinos that undergo parametric oscillation and Mikheyev-Smirnov-Wolfenstein[47] as they pass through the earth. This way is used in PINGU[48].
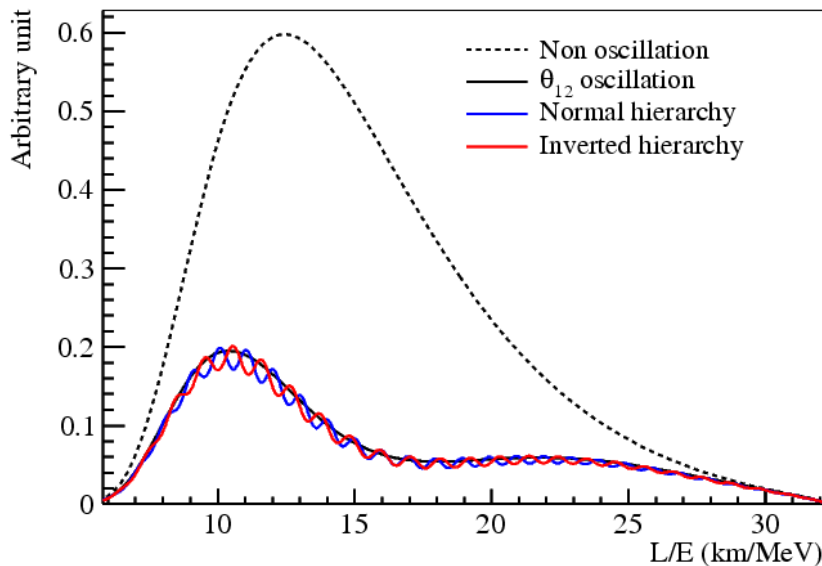

Figure 3: Here the neutrino oscillation can be seen, based on the different mass hierarchies in relation to the length over the energy. The dotted line shows the expected curve for a non oscillating particle, the black the normal oscillation shown in the first two terms of equation (15). The red now shows the oscillation for the inverted mass hierarchy after equation(17) and the blue the normal hierarchy(16)[7].

2.2 JUNO-Experiment

The JUNO Experiment is a multi purpose neutrino experiment with a focus on the determination of the neutrino mass hierarchy. The knowledge of the mass hierarchy can lead to many new discoveries in astro and astroparticle physics. In chapter 2.2.1 the general detector layout and basic facts about the JUNO-Experiment will be discussed. Chapter 2.2.2 deals with other measurements which JUNO could be used for. At last in chapter 2.2.3 the contributions of the university of Hamburg will be mentioned.

2.2.1 General Data and Detector Layout

The Jiangmen Underground Neutrino Observatory (JUNO) is a multipurpose experiment with the determination of the mass hierarchy as its main goal. The mass hierarchy has a fundamental role in astronomy, cosmology. It can also be an important factor to measure the CP-violating phase. Furthermore it can give a clue for a better understanding whether the neutrino is a Dirac or a Majorana particle.

The testing site is located $700\,\mathrm{m}$ underground near Kaiping City in the Greater Jiangmen region in China. The measurements are achieved by the use of reactor anti electron neutrinos. A way to measure the $\bar{\nu}_e$ is using the inverse β-decay. The positrons react with the electrons in the surrounding area creating a pair of photons. After $200\,\mu$s on average the neutron leads signal via neutron-proton capture. The combination of these two signals leads to a distinct anti neutrino signal. By observing the energy spectrum of the anti electron neutrinos it can be determined, which mass hierarchy is at hand. Using equations (16) and (17), it can be determined, which mass hierarchy is correct. The anti electron neutrinos will be produced by the power plants Yangjiang and Taishan with a planned thermal emission of $36\,\mathrm{GW}$, as nuclear power plants are the best understood, controllable and intense source for anti neutrinos. During the beta decay of ^{235}U,^{238}U,^{239}Pu, ^{241}Pu six anti electron neutrinos are produced per fission[9]. For the optimal $\frac{L}{E}$ factor of $11\,\frac{\mathrm{km}}{\mathrm{MeV}}$to distinguish the two mass hierarchies the power plants are both $53\,\mathrm{km}$ away from the testing site. The location of the testing site on a map can be seen in figure 4.

The detector is made out of three parts: the central detector, a cherenkov detector and a muon tracker. The central detector is an acrylic sphere with an inner diameter of $35,4\,\mathrm{m}$ and will use $20\,\mathrm{kt}$ of Linear Alkyl-Benzyne (LAB) liquid scintillator, thus making

Figure 4: The location of the JUNO testing site is in Jinji town, Kaiping city, in the Greater Jiangmen region [29].

it a LAND (liquid scintillation anti neutrino detector). To improve the signal output $3 \frac{\text{g}}{\text{L}}$ PPO will be used as fluor. $15 \frac{\text{g}}{\text{L}}$ of Bis-MSB will be added to the liquid scintillator as a wavelength shifter, to shift the wavelength to an area where the PMTs are more sensitive. The stainless steel lattice has a diameter of 40 m leaving room for a buffer zone. The buffer consits out of water and is directly connected to the water from the overall tank. The stainless steel lattice harbors 18000 20-inch and 25000 3-inch PMTs. The PMTs have to be protected from implosion by acrylic covers and are made by Hamamatsu and Norther Night Vision Technology (NNVT). To resolve the mass hierarchies and the oscillations shown in figure 3, the detector is must have a resolution of 3% at 1 Mev and the PMTs must have a photon detection efficiency at a level of 30% [19]. To improve the time resolution the spaces between the 20-inch PMTs will be filled with 3-inch PMTs.

The central detector is surrounded by a cylindrical tank filled with 20 kt of water. This prevents outside radiation from interacting too much with the central detector, but also serves as a cherenkov detector for cosmic muons. For this, 1500 veto PMTs will be placed at the edge of the tank. The muon detection efficiency will be 99.8% through the use of tracker elements from OPERA. The tracks from the muons will then be used to veto these signals out. The entire detector will be shielded from the magnetic field using two coils. Additionally some of the veto PMTs will be shielded as well using μ-metal cages around the individual PMT[35]. The whole detector will be accessed and calibrated through a

17

shielded chimney connected to the surface. An Overview of the complete detector is given in figure 5. JUNO is a high precision experiment, thus knowing the background and shield-
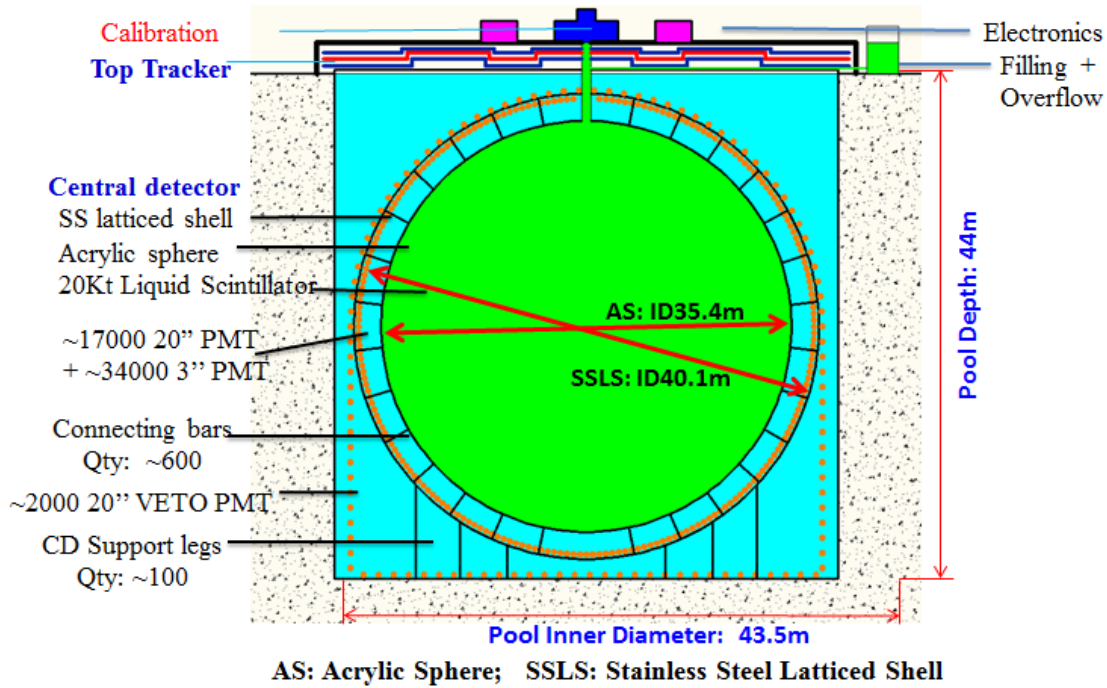

Figure 5: This picture shows a systematical overview of the whole detector. In the middle is the inner vessel with 20 kt liquid scintillator, a stainless steel lattice with 18000 20-inch PMTs surrounded by a water tank. On top of the water tank the muon tracker from OPERA can be seen [44].

ing the experiment from the background as good as possible is essential. The underground build of the experiment and the usage of veto detectors are used to shield it from the muonic background. Most of the background is so called *accidental background.* This is radioactive background from the PMT glass, the surrounding rocks, neutrons and cosmic isotopes. Additionally the decays from the Uranium and Thorium chain can influence the measurements in two ways. The α-particles from α-decays can interact with the ^{13}C inside the liquid scintillator material. If the neutron is fast enough or there is a gamma from the de-excitation of the ^{16}O excited states, this interaction results in a minor background of 0.001 to 0.005 signals per day. The β-decay inside the earth creates other neutrinos so called geo-neutrinos, which will interact with the material the same way as the reactor neutrinos. This provides us with a background of 1.5 signals per day on average. Cosmic isotopes like ^{8}He and ^{9}Li can be created, when cosmic muons interact with the ^{12}C in the scintillator. These cosmic isotopes are unstable via the β-decay they can exhibit neutron unstable states with a branching ratio of 16% and 51% respectively. The neutron unstable

states emit a neutron and a photon upon their decay. This photon is mainly captured by hydrogen. Together with the photons produced by the electrons from the β-decay, the signal is indistinguishable from reactor anti neutrino signals. This would result in a background of 1.6 signals per day with the veto already used.

2.2.2 Additional Measurements

Aside from the mass hierarchy the JUNO-experiment can be used to gain knowledge about other neutrino related phenomena. This includes the measurement of three other oscillation parameters (Δm_{12}^2, Δm_{23}^2 and $\sin^2(\theta_{12})$) with an unprecedented uncertainty of less than 1%[10][11]. This is due to the high statistic and precision that has never been achieved before.

Also the measurement of geoneutrinos can give an insight into the distribution and amount of natural radioisotopes within the earth. This will result in a better understanding of the radiogenic heating of the earth and so the whole heating mechanism as the heat balance of the earth depends on the decay of these radioisotopes. This has already been done at KamLAND and Borexino[49], so JUNO would further increase the statistics and lower the relative uncertainty, which is too high to distinguish the two most important geoneutrino models. Also JUNO could be under completely different geographical influences as them, because Borexino is located on the other end of the eurasian continental plate and KamLand is close to the edge of it. So the measurement of geoneutrinos at JUNO can give insight in geographical phenomena. As this is just a short preview of the topic, [22] can give additional information about geoneutrinos.

Solar neutrinos were the key factor to determine the neutrino oscillation. While it was observed that the overall neutrino flux was similar to the expectations, the flux of the electron neutrinos showed a deficit. The JUNO-experiment may answer the two remaining questions about the solar neutrino spectrum. The first would be the measurement of solar neutrinos from the CNO-cycle. With this the metalizity of the sun could be verified. The second is the measurement of the oscillation probability of solar neutrinos with an energy between $1\,\mathrm{Mev}$ and $3\,\mathrm{MeV}$. The measurements for neutrino events with an energy under $1\,\mathrm{Mev}$ have been conducted and show the oscillation probability expected for neutrinos in vacuum. Events with an energy greater than $3\,\mathrm{MeV}$ show the expected probability for oscillation in matter according to Mikheyev-Smirnov-Wolfenstein. The area between those

two is interesting as it could prove if the theory behind the Mikheyev-Smirnov-Wolfenstein effect is correct, because it assumes continuous transition from one oscillation probability to another. Further information on solar neutrinos are given by [18].

Neutrinos also have a fundamental role in supernovae. 99% of the energy of a core-collapse supernova is radiated in form of neutrinos. By carrying the energy from the core to the surface of the star they are important for the successful explosion. Supernovae happen statistically every few centuries with a distance of around 10 kpc. A supernova in this distance would lead to JUNO measuring 5000 neutrino signals in a few seconds. These can be measured, because the PMTs have an internal memory. This will give insight in the energy spectrum and mechanisms behind supernovae. As neutrinos of a supernova reach earth before the light, JUNO can be used to warn the astronomers that a supernova is coming. Also the combined neutrino flux from earlier supernovae can be measured giving an insight in the star forming rate. For further information about super novae neutrinos [17] can be read.

The knowledge about the proton decay can give inside in the asymmetry between matter and antimatter, because the baryonic number needs to be violated to explain it. The most favoured proton decay mechanism is $p \rightarrow K^+ + \bar{\nu}$ and is currently tested in Super-Kamiokande [33]. Because the Kaon (K^+) is just underneath the cherenkov-border in water, the Super-Kamiokande-experiment does not have a high resolution for measurements involving Kaons. But this does not count for JUNO as it uses liquid scintillators. That is why JUNO is expected to have a three times better sensitivity than Super Kamiokande for the most favoured proton decay channel. Further Information are given in [33]

2.2.3 Contribution of the University of Hamburg

The university of Hamburg mainly focuses its efforts for JUNO on two things. First of is the construction of an photomultiplier test facility. Because of the high quality demand each of the 20000 20-inch PMTs will be tested twice. First as a general control and later to create a databank about the sensitivity of the of the sensors and the dark current. The test facility will be composed of four magnetic shielded containers, which each have 36 aluminum drawers. Every drawer is filled with one PMT. This way 144 PMTs could be tested at the same time using the data acquisition (DAQ) developed in Eberhard Karls University Tübingen. The containers will be discussed further in chapter 3.2.

The second focus is the software development for the reconstruction of 3D topologies. This is motivated from the development of new methods to get information about the 3D-particle tracks and the loss of energy within the topology. These methods allow for the first time to measure any topology independent of the hypotheses. These methods were developed during the involvement of University Hamburg in the LENA-group. Inside JUNO the events these methods are applied to will be low energy (MeV) and high energy (GeV) events. Of these the primary focus will be on GeV muon events.

2.3 PMT-Physics

Nowadays a lot of experiments depend on the measurement of photons. The most detectors used for these experiments use the photoelectric effect to transform a photon into an electron. Photomultipliers are used to see single photon events with low energies. The photomultipliers used in the JUNO experiment are the photomultiplier tubes (PMT). This is why they will be further discussed in this chapter. In chapter 2.3.1 the general idea of how PMTs work will be discussed. Chapter 2.3.2 the signals without an external light source in front of the PMT will be explained. Thereafter in chapter 2.3.3 the influence of magnetic fields on PMTs will be explained.

2.3.1 Working principle of PMTs

A photomultiplier tube (PMT) is always composed out of the same three components, a photocathode, an electron multiplier and an anode, all within an evacuated glass tube. The basic principle is that an incoming photon hits the photocathode resulting in a free electron because of the photoelectric effect. This electron will then be accelerated towards the electron multiplier by an electric field. There are different ways of how they multiply electrons. The most common way is to use dynodes, which is the specific name for electrodes within a PMT. After striking the first dynode the electron releases multiple other electrons. These electrons are now drawn towards the next dynode because they are held at increasingly higher potentials through the use of voltage dividers. Because every electron produces multiple free electrons upon hitting a dynode, this results in an exponential relation between the number of dynodes n and the number of secondary electrons detected at the anode M:

$$M = m\delta^n \tag{18}$$

where m is the number of photoelectrons impinging the first dynode and δ is the secondary electron emission. It is the number of released electrons over the number of incoming electrons for one dynode, which depends on the voltage applied to the dynode. The factor that connects M and m is called gain. The gain is typically around 10^7, but strongly varies based on the model and the supplied voltage[37]. The way of multiplication and a schematic overview of a dynod PMT is given in figure 6 .
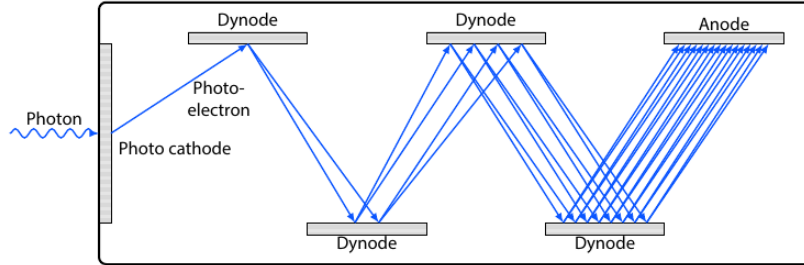
Figure 6: This is an schematic overview of the working principle of a dynode PMT [13].

Another way to multiply the electrons in a PMT is to use microchannel plates. That is why this kind of PMTs is referred to as microchannel plate PMTs (MCP). The plate is made out of many glass capillaries (channels) in parallel bunches. To have the right secondary emission properties and electric resistance each capillary has an inner radius of 3-10 μm. Each channel is an independent electron multiplier. The composition of an MCP-PMT and its way of multiplication can be seen in figure 7. The moment an electron hits the inside of a channel, secondary electrons are emitted. On their way through the channel the electrons hit the walls many times, resulting in more and more secondary electrons to be emitted, as the electrons are steadily accelerated to have enough energy to do that. The acceleration is done by an electric field, which is formed by a voltage applied from the input electrode of the PMT to the output electrode. Because the opposite sides of a channel are closer than the dynodes of a dynode PMT a high resolution for the usually smaller size is possible. The number of secondary electrons detected by the anode for this type of PMT is given by [12]:

$$M = me^{\alpha\delta}. \tag{19}$$

Where α is the length to diameter ratio $\left(\frac{L}{2R}\right)$ and δ is again the secondary electron emission, but this time it is not dependent on the applied voltage, but just on the selected wall material.

Because some photons do not release a photoelectron and not all of them are going to impinge the first dynode or an inner wall of a capillary, the parameter m is not equal to the number of incident photons s. Their correlation is given by
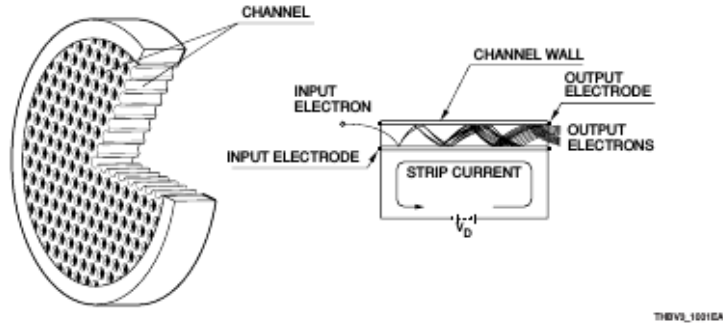
$$s\Psi(\lambda) = m. \tag{20}$$

23

Figure 7: On the left a picture of the MCP PMT can be seen. The right picture shows the way of multiplication [12].

$\Psi(\lambda)$ is the photon detection efficiency with

$$\Psi(\lambda) = \alpha\eta(\lambda). \tag{21}$$

Here $\eta(\lambda)$ is the quantum efficiency, which is the number of emitted photoelectrons per photon. It depends on the wavelength as photons with big wavelengths will not have enough energy to create a photoelectron. If the wavelength is small, it is more likely for the photon to be absorbed by the glass and so it can no longer interact with the photocathode. Because of this PMTs have a spectral range from around 300 to 650 nm with the quantum efficiency reaching its maximum of about 0.3 at circa 420 nm dependent on the model[38][42]. Where α is the probability for the photoelectron to hit the first dynode, called collection efficiency. It usually has a values slightly lower than 1. So for most cases it is a good approximation to use $\Psi(\lambda) = \eta(\lambda)$.

The transit time is the time interval between the arrival of a light pulse at the photocathode and the appearance of the output pulse. The fluctuation of the transit time is another key factor for PMTs called the transit time spread (TTS). The TTS is usually expressed as the FWHM, but can also be expressed as the standard deviation. If the histogram shows a Gaussian distribution, the FWHM is equal to 2.35 of the standard deviation. Because MCP-PMTs are shorter, the TTS is also smaller for them. MCP-PMTs, with size of $756\,\text{mm}^2$, have a TTS of 70 ps, while dynode PMTs with a comparable size of $633\,\text{mm}^2$ have a TTS of more than 170 ps[42][43], the TTS in both measurements were determined with the FWHM. The MCP-PMTs used in the JUNO experiment do not show this behavior as they use a special mechanism to increase the quantum efficiency. These 20-inch PMTs show TTS of 12 ns, while 20-inch dynode PMTs have a TTS of 2.8 ns[50].

The anode of a PMT is actually an electrode that collects the previously multiplied electrons and transforms them into an electron current to an external circuit.

2.3.2 Dark current

Even without an external light source the PMT still has an output signal. This signal is referred to as dark current. To allow high precision measurements it has to be kept as low as possible. The dark current spectrum changes with the supply voltage as different effects dominate for different voltages.

The so called leakage current is most prevalent in the low voltage region. This is caused by an insufficient insulation material, because PMTs operate at high voltages of 500-3000 V [12], while the signal current is low with I<100 μA. The Ohm's Law gives the connection between the leakage current and the other parameters.

$$I = I_{supp} + I_{leak} = \frac{U}{R} \tag{22}$$

Where I is the current, I_{supp} stands for supplied and I_{leak} for the leakage current. As standardized, U is the voltage and R the resistance. The effect becomes stronger, if dirt gets on the glass stem, socket or base.

The medium supply voltage region has the best signal to noise ratio. The dominant effect here is the thermionic emission. For photomultipliers to be effective the work force for an electron to escape has to be low, so that even low energy photons can be detected. But this means that the thermal stimulation at room temperature can also cause electrons to be emitted from the photocathode and the dynodes. It mainly depends on the photocathode, because it is bigger then the dynodes and because of the multiplication the dynodes get less and less relevant the further they are. The thermionic emission is described by [12][53]:

$$I = AT^2 e^{\frac{-W}{k_B T}}, \tag{23}$$

where A is the Richardson constant and W the work function of the photocathode material. The work function is the energy difference between the Fermi level and the vacuum level. k_B the Boltzmann constant and T the temperature.

For high voltages two effects are dominant, the field emission and the scintillation of both the glass and the electrode support materials. The field emission is the abrupt dark current increase by electron that are freed from the dynodes. This happens because of the high electric field rooted in the extreme voltage. A maximum supply voltage for PMTs is given because this effect damages it. The glass and electrode support scintillation is based on electrons that do not account for the output signal as they strayed from the intended path and missed the first dynode. Those electrons can then hit the glass causing a direct radiation, which results in pulses, which will be detected later then expected. This effect can be reduced by using a conduit paint around the outside of the glass bulb.

The afterpulse is an effect occurring, because of residual gases inside the tube. Molecules inside them can be ionized by the electrons on their way to a dynode. When a positive charged ion strikes the first dynode or photocathode, they will produce a lot of secondary electrons causing a second signal. Because they need a signal to produce this noise is called afterpulse. The the typical darkcurrent spectrum is shown in figure 8 via the dotted line. It is mostly dominated by thermal electron emission. This causes the spectrum to be focused more in the lower pulse height region as thermal electrons usually get multiplied less.
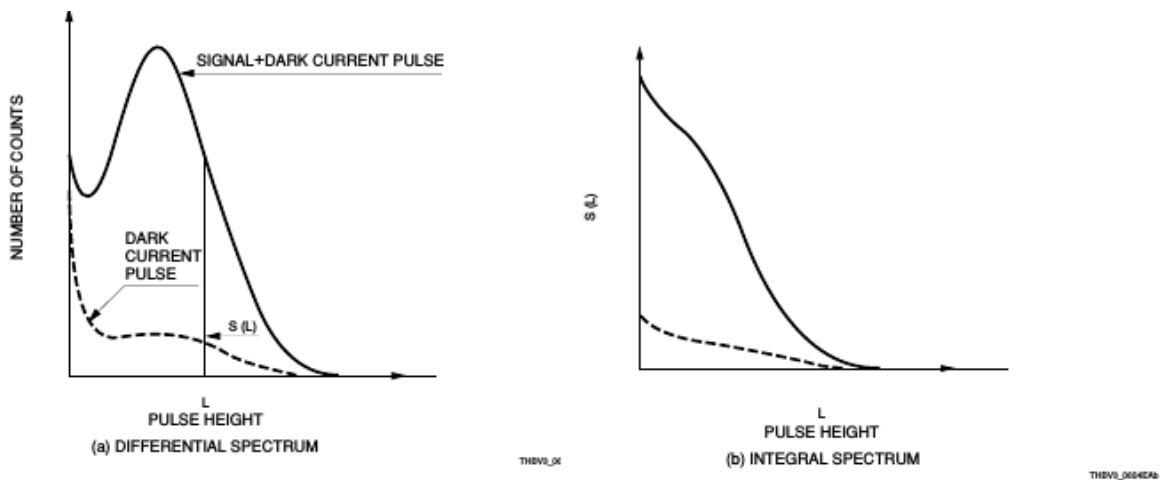

Figure 8: The dotted line shows the typical dark current spectrum. It is mostly dominated by thermal electron emission. This causes the spectrum to be focused more in the lower pulse height region as thermal electrons usually get multiplied less [12].

The last kind of noise is caused by the environment. Astronomical radiation like muons

can cause Cherenkov-light while passing through the glass as muons are faster then light in this medium. Also the radiation from radio isotopes in buildings and most glasses causes problems. But these influences are negligible in contrast to the others.

2.3.3   Influence of magnetic fields on PMT Measurements

Because electrons travel through the PMT with low energies, measurements are affected by magnetic fields. The path the electrons travel, can be derived via solving the differential equation, which is made by using Newtons second law and the Lorentz force:

$$m_e \ddot{\vec{r}} = e(\vec{E} + \vec{v} \times \vec{B}), \tag{24}$$

here m_e is the mass of the electron, e is the elementary charge, $\ddot{\vec{r}}$ is the acceleration, $\vec{v}$ is its current speed, $\vec{E}$ is the electric field and $\vec{B}$ is the magnetic field. This force is responsible for transporting the electrons from the photocathode to the first dynode, at least in the electromagnetic field that the PMT was produced for. In case of a big difference between the planned field and actual field, the electrons miss the first dynode resulting in a higher glass scintillation and less total signals. The effect grows stronger for PMTs with a longer distance between the photocathode and the first dynode and for a smaller first dynode opening. Which is why MCP PMTs have usually a higher tolerance for strong magnetic fields. The anode sensitivity of most dynode PMTs with a glass front as the ones used in the JUNO experiment will be reduced by 50% by a magnetic flux density of circa $0.1 \, \mathrm{mT}$[12]. This reduction of the efficiency make it necessary for the JUNO detectors to be shielded from the external magnetic fields. Furthermore the test stands have to be shielded to calibrate the PMTs and their background noise.

A potential PMT candidate for the JUNO experiment was tested by [19] at different magnetic fields, with the PMT oriented along the magnetic field vector. The results show that the PMT performs just fine at a magnetic flux density of only $10 \, \mu\mathrm{T}$. But for $20 \, \mu\mathrm{T}$ it starts to fail the required homogeneity of photon detection efficiency greater than 15% and has an an average photon detection efficiency of less than 24%.

3 Commissioning

This section consists of two smaller chapters and a catalog of the used instruments. The first chapter 3.2 deals with the test facility that will be send to China and the efforts to minimize the magnetic field inside to minimize the negative effect discussed in chapter 2.3.3. The chapter 3.3 deals with the measurements in the small optical test stand. In chapter 3.1 all the instruments used for the various measurements will be discussed.

3.1 Means of Measurements

This chapter is a small catalog of all the used instruments used for the measurements.

3.1.1 Magnetic Field Measurements

To measure the magnetic field the magnetic field sensor FLC3-70 from *Stefan Mayer Instruments* was used. It can measure the magnetic field up to $200\,\mu$T[23] in all three dimensions at the same time. The data can be received using the read out software HTerm. Because the data is given in form of corresponding channels, the channels needed to be calibrated. This was done by University Aachen [13]. With the calibration the absolute value of the magnetic field is given by:

$$|B|[\mu T] = 3.28 * 10^{-3}\sqrt{c_x^2 + c_y^2 + c_z^2} \tag{25}$$

With |B| being the absolute value of the magnetic field in μT. C_i refers to the channel that is given out in direction i.

3.1.2 Small Laboratory

Here are all the measurement tools used in the chapters 3.3.2, 20 and 3.3.4.

- The power supply of the PMT is a CAEN Mod. 1470. With it the voltage and current given to the PMT can be changed. Because of problems in the past the power supply is in a different crate as the other instruments.

- For the measurements inside the small laboratory test facility a two-inch R1828-01 PMT was used. It has a borosilicate glass tube and a spectral response range from 300 to $650\,$nm. The photocathode is composed out of a bialkali material. The PMT

has twelve linear focused dynodes and an operating temperature of -30 to 50 °C. The maximal supply voltage that can be used is 3000 V [45].

- To read out the data from the PMT with a computer it is required to use an Analog to Digital converter (ADC). The one used in the small test facility is CAEN Mod. N957. It has a 8k-Multi-Channel. The incoming pulses can be of any shape as long as they are in the range of 0 to 10 V and have a rise time of at least $0.1\,\mu$s [21]. The ADC has an internal threshold that behaves exponentially and can be set between 0 and 99, with 0 being the lowest threshold. All measurements were conducted with a threshold of 0.

- Because the ADC needs positive signals and the negative signals from the PMT need to be inverted. Upon testing the different instruments that could do so, it was discovered that the amplifier from Ortec deforms the signal the least. For all detected signals to be converted, the amplifier was used to its full extend. This meant that the signals input Voltage increased by 20 fold.

- The signals from the PMT were checked using the Oscilloscope MSO 4104.

3.1.3   Coincidence Circuit

These are the tools only used for the coincidence measurements in chapter 3.3.4. A schematic overview of the coincidence is given in 24.

- The pulses given to the LED were generated by the pulse Generator (Agilent 81130A). The pulses from this generator have a frequency range of 170 kHz to 660 MHz. The produced signal has a voltage between 100 mV and 2.5 V[24].

- The LED used for the measurements is a G-Nor GNL-3014BC-1. It is a blue LED, which can be bought at any electronics store. Thus the light intensity of the LED is unstable.

- For the LED-measurements the amount of signals from the PMT were reduced using the discriminator CAEN Mod. N844. The threshold of this discriminator can be programmed between 1 mV and 255 mV in 1 mV. The discriminator needs a minimum absolute value of the signal voltage of 3 mV to detect a signal. Also signals over 400 mV or under -400 mV cannot be detected[39].

- The pulses from the pulse generator were amplified and split into two for our circuit by the amplifier CAEN Mod. N978. For splitting the signals in to both of its outputs are used. It amplifies both negative and positive signals by 0 to 10 times if they are between -6 and 6 V[40].

- One of those output signals was then used to open a gate via the dual gate generator LeCroy Mode 222. The input signal needs to be between 100 mV and -5 V.

- The gated signal and the signal from the PMT are both put into the quad coincidence logic unit CAEN Mod. N455. It has both an *and* and an *or* function. The *and* function used in this experiment only lets a signal through, when both signals are measured at the same time. For this the signal from the pulses had to be gated for a coincidence circuit, because the PMTs signals from the LEDs light are normally distributed around a specific time after the pulse. The delayed time is dependent on the distance between the LED and the PMT and the length of the cables used. The incoming signals need to be between 0 to -50 mV and -600 to -800 mV for the different logic entries, which is the NIM-standard[41].

- To count the number of coincidences and generated pulses the scaler CAEN Mod. N1145 was used.

3.2   Magnetic Field

The JUNO PMTs will be tested and calibrated inside shipping containers with a Heat, Ventilation and Air Conditioning (HVAC) unit. The containers have an inner height of 2.5 m, the distance from the left wall to the right one is 2.25 m. The distance between the door at the front and the HVAC at the back is 6 m. Because the performance of PMTs can be influenced by magnetic fields as described in chapter 3.2, the JUNO detector and the test facility need to be shielded against the magnetic field of the earth. The shipping containers were shielded against the magnetic field by alternating layers of silicon soft iron and aluminum sheets. Silicon soft iron is a material that consists usually out of 96% iron and 4% silicon [52]. Soft iron is a ferromagnetic material. These materials have have a high relative permeability μ_r. The permeability μ is the is the ability of a material to support the formation of a magnetic field inside the material. The relative permeability is the permeability of the material divided by the permeability of vacuum $\mu_0 = 1.257 \text{V s A}^{-1}$ m^{-1} [51]. Soft iron has a relative permeability of 7000, mild steel has a relative permeability of 800-2000 as a comparison. Because of the high permeability the magnetic field flows through the container walls instead of flowing through the interior. To ensure the magnetic field is below 10% of the earth,s magnetic field for the PMTs to work properly, the magnetic shielding had to be tested using the magnetic sensor discussed in chapter 3.1.

A measuring lattice was designed for the container. The points had a height of 0, 75, 150 or 225 cm from the floor of the container. The distance of the points to the left side of the container was either 0, 83, 166 or 250 cm. The distance to the door changed in steps of 90 cm, expect for under 90 cm and over 560 cm as they were close to the weak points of the container. Namely the door and the HVAC unit. At these points the distance from the points to the door was changed in 20 cm steps. The position of all the points has an uncertainty of 2.5 cm, because the tools used to measure the position were put away during the measurements. This was done to ensure that the magnetization of the tools had no influence on the measurment. At every point of this lattice the magnetic field was measured using equation(25). Then the magnetic field was plotted with gnuplot. On these plots it was hard to distinguish between magnetic fields meeting the requirement and larger magnetic fields. To overcome this a colour code was created. Black or 1 for magnetic fields that easily meet the requirements. These points have a magnetic flux lower than $4\,\mu\text{T}$. Violet or 2 for magnetic fields that barely meet the required $4.5\,\mu\text{T}$. This means they had a magnetic flux ranging from 4 to $4.5\,\mu\text{T}$. Orange or 3 is for magnetic fields that have a flux
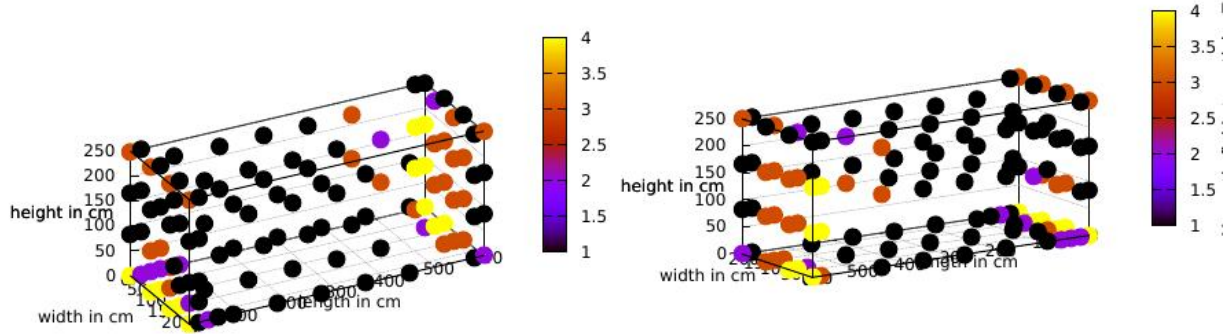
Figure 9: This picture shows the measurements of the magnetic field in side the second container. Because of the range of the magnetic field the points of a magnetic field that fit the requirements are not so easy to distinguish from magnetic fields that are twice as high. To overcome this a colour code was created. Black or 1 for magnetic fields that easily meet the requirements. The have a magnetic flux lower than $4\,\mu$T. Violet or 2 for magnetic fields that barely meet the required $4.5\,\mu$T, so from 4 to $4.5\,\mu$T. Orange or 3 is for magnetic fields that have a flux between 4.5 and $7.5\,\mu$T. These points will probably not cause a problem for the testing. The points marked in yellow are points, where the magnetic field will most likely influence the measurements. These points have a magnetic field flux of more than $7.5\,\mu$T. On the left is a picture of the container with the backside in the left side. The front of the container faces the left side of the right picture.

between 4.5 and $7.5\,\mu$T. These points will probably not cause a problem for the testing. The points marked in yellow are points, where the magnetic field will most likely influence the measurements. These points have a magnetic field flux of more than $7.5\,\mu$T. The magnetic field of the second container can be seen in figure 9. On the left is a picture of the container with the backside on the left side. The front of the container faces the left side of the right picture. As the measurements showed that the containers did not fulfill the requirement of being lower than $4.5\,\mu$T, the company in charge of producing the containers had to enhance the container. The magnetic field of the container after it was improved can be seen in figure 10. Here only the magnetic field at the left door was measured as only this door was improved. So the effects on the back are deemed negligible and the middle was already good enough so the improvement there was not interesting. Also as the magnetic field in the middle has to come from the outside, so if the magnetic field on the outer parts of the container is alright so will the inside. The points had a distance to the door of 10 or $30\,$cm and heights of 30, 90, 150 or $210\,$cm. The distance of the points to the left wall were 0, 30, 60 or $120\,$cm. As the point with the highest magnetic flux was under $7\,\mu$T after $10\,$cm and under $4\,\mu$T for a distance of $30\,$cm to the door the colour code was not used, instead the magnetic flux was plotted using its value in μT. Because
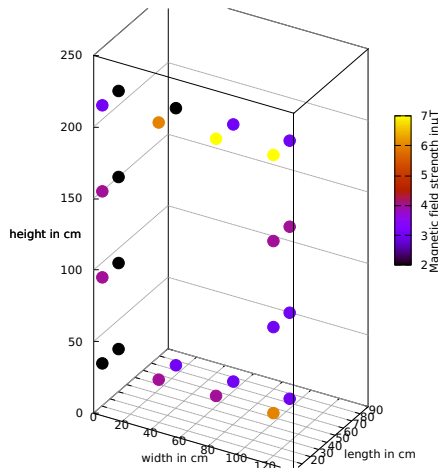
Figure 10: This picture shows the magnetic field on the left door after the improvement. This side needed to be reinforced, because the left side is where the measurements will be conducted. As this measurement did not require the use of the colour code, it was not used.

the magnetic field of the second container was not as low as required and because it was reported that the first container after the arrival in China had a much larger magnetic field than in Hamburg, the magnetic fields inside the third and fourth container were measured in Berlin and later in Hamburg. These measurements indicated that even on the short tour from Berlin to Hamburg the container's magnetic flux increases. This can be caused by magnetization or by the shielding getting damaged. The plots of the magnetic fields can be seen in figure 11. The points measured in Berlin all had a distance from the door or the back of 10 cm, because they were already good enough it was not necessary to look at the magnetic field of the other points in detail. The measured points had heights of 0, 60, 120,180 and 180 cm. And the distance to the left wall was 0, 120 and 250 cm to measure it in the middle and the two sides were the door opens. The measurements in Hamburg were taken with the same heights as the improved front. The distance to the door or the back are 10, 30 and 60 cm. The measured points had a distance to the left wall of either 0, 60,120, 180 or 240 cm. Because the front was especially affected by this change, the left side of the door was enhanced with a fine matt foil for magnetic shielding. This is also an important test to see, if there is a easy and fast way to reduce the magnetic field in China, as the company can not go to China to fix the container like in figure 10. The influence of the enhancement can be seen by comparing the pictures seen in figure 12. On the left the front of the 3rd container as measured in Hamburg is shown and on the right is the same container with the magnetic foil. The fine matt foil only covers the three columns on the left, which is why no improvement on the right side of the door can be seen. This shows
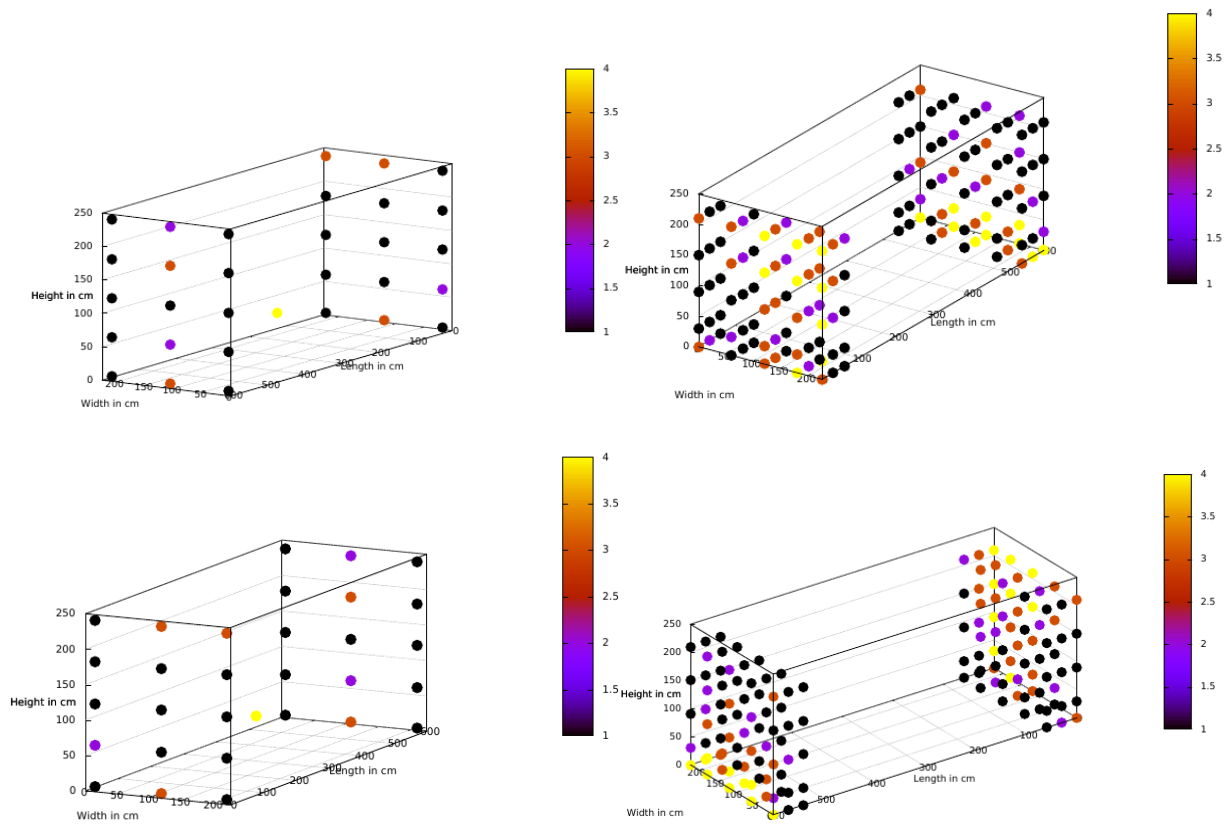
Figure 11: The left pictures show the measurements taken in Berlin and the right the ones from Hamburg. The pictures on top show the magnetic field seen from the front and the bottom ones show them with the backside in the front. This picture uses the same colour code as in figure 9 . As the measurements in Berlin were so good that there were no yellow points, one was put in the middle of the left pictures, so gnuplot would not change the colour scheme.

that most of the points in the relevant area are now in the required range, which leads to believe that it is a quick way to solve the magnetic field problem in China. As no point under the cover shows a magnetic flux, which is likely to influence the measurements, this impression is further increased. For a direct comparison the magnetic field was measured at the same points as the measurements in Hamburg in figure 11.
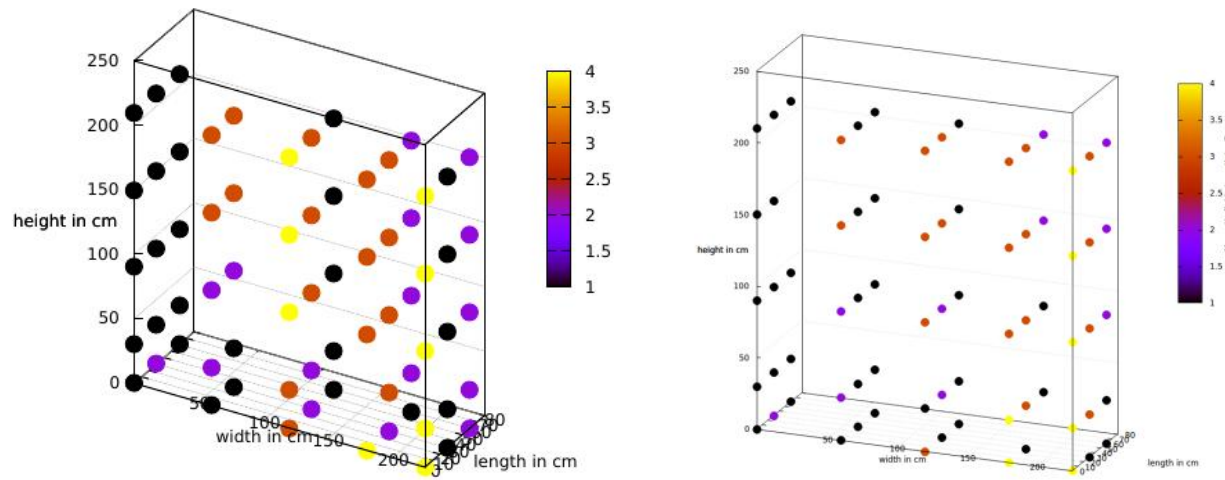
Figure 12: On the left illustrates the magnetic field of the front of the container without any reinforcement measured in Hamburg. The picture on the right show the magnetic field after fine matt foil was applied to it. The pictures use the same colour code as previously mentioned.

3.3 Laboratory PMT test facility

The measurements done in this section were done with the PMT inside a wooden box. The wooden box was used to protect the PMT from the light. This effect was further increased by the coverage of the box with black PVC foil. The box is placed on a wooden support structure. It can be opened with a wooden handle. To guarantee that it is closed, metal clips connect the top and front of the box. The box has the outside dimensions of $179.5\,\text{cm}\times62\,\text{cm}\times66\,\text{cm}$. A schematic overview is given in figure 13.
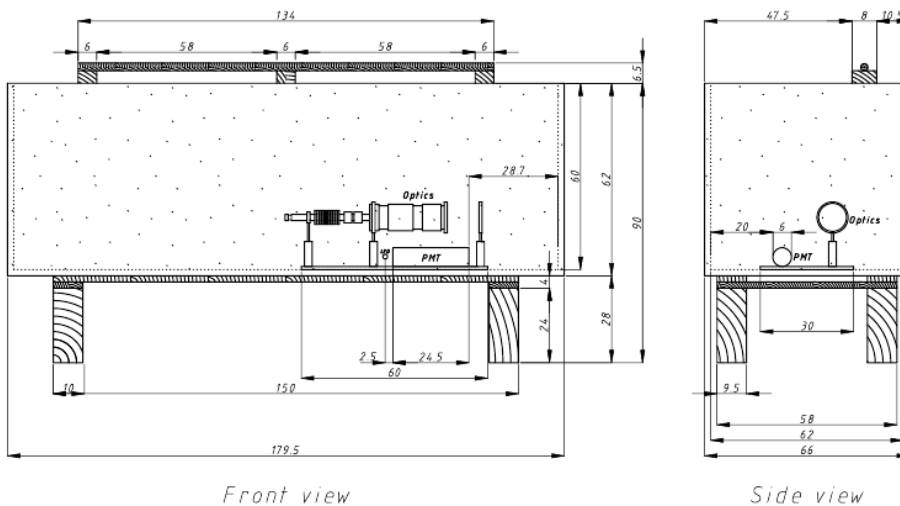
Figure 13: systematic overview of the PMT inside the wooden box. The box was placed on a wooden support structure. It can be opened with a wooden handle. To guarantee that it is closed, metal clips connect the top and front of the box. On the right the view of the PMT is shown from the side[13].

3.3.1 ADC test

To understand the spectrum plotted by the ADC better and directly plot the number of events in dependency on the output voltage of the PMT, the pulse generator was directly plugged into the ADC. A linear regression was made by increasing the voltage of the pulses in $100\,\text{mV}$ steps and looking at the corresponding channel 14. The output voltages have been verified using the oscilloscope.
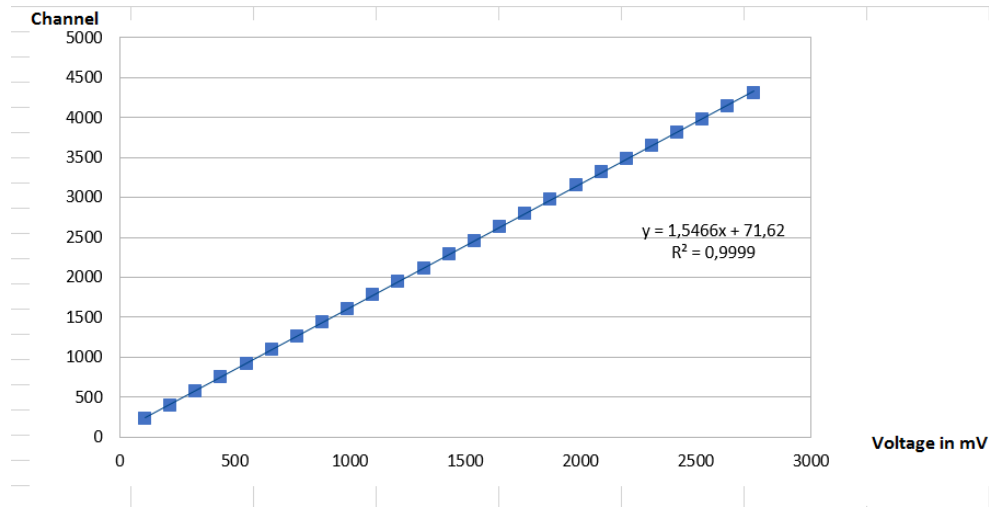
Figure 14: Linear regression of ADC-channels in dependency of pulse voltage.

In figure 14 can be seen that it does not act like it should. The used ADC has a gain error and an offset. Because the expected relation between the voltage and the ADC channel for an ADC with a range from zero to 10V in 8000 channels should be:

$$C = 0.8U[\text{mV}] \quad \text{instead of the measured} \quad C = (1.55 \pm 0.01)U[\text{mV}] + 71.62 \pm 5.51 \quad (26)$$

Here C is the responsible channel for the input Voltage U in mV. This is a big difference to the expectation, but the influence of these errors on measurements is not that big if they are known to the one conducting the measurements.

3.3.2 Dark Current Rate

The measurements in this chapter were conducted with only the 2-inch PMT inside the box. The signals of the PMT needed to be inverted and strengthened to properly read them out. The signals need to be amplified, because the signals from the PMT are all in a small range. As each channel has a small uncertainty, the amplifier was set to multiply the by twenty fold, to keep the influence of a channels uncertainty as low as possible. This gain was tested with the pulse generator and the oscilloscope. These signals were then translated by the ADC and sent to the Computer for read out. The electronic setup can be seen in figure 15, where the amplifier is marked as AMP.

PMT $\longrightarrow$ AMP $\longrightarrow$ ADC $\longrightarrow$ PC
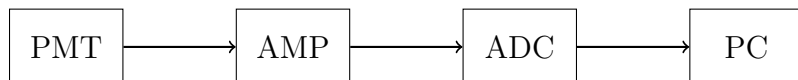
Figure 15: This is the setup for dark current Measurements. Here AMP stands for amplifier.

In the beginning the dark current rate was higher. After taking out the old PMTs the dark current rate dropped by half. This can be seen in figure 16. These measurements were taken with a suply voltage of 2450 V. There the blue line shows the spectrum before the PMTs were taken out and the red line after. This shows that the second peak completely vanishes and the first one shrinks. As the second peak corresponds with signals from the LED 18, this noise is likely to be caused by the old PMTs acting as an antenna. As this effect was observed at a time when Petra III was inactive. Also a the possibility of a discharge by the foil can eliminated, because when a similar effect began to show measurements with and without the PVC foil were conducted. Additionally the foil was scrubbed with metal. All of this had no effect. The crate creates a high frequency noise after being started. This noise was avoided by letting the crate run for multiple hours before conducting a measurement.

The dark current spectrum was taken in dependency on the supplied voltage. The PMT started taking data at 1800 V, from there the dark current was measured by increasing the voltage in 100 V steps. The measurements were taken over at least fifteen hours. Using the *.root* file, which the ADC automatically saves, the measurements were normalized on their frequencies and the corresponding channel was substituted by the voltage of the signal using the measured relation from figure 14 and equation(26). The measurements can be seen in figure 17. The picture on the left shows the same spectrum, but the range of the y-axis is set higher. This way the focus is more on the first peaks and it shows that
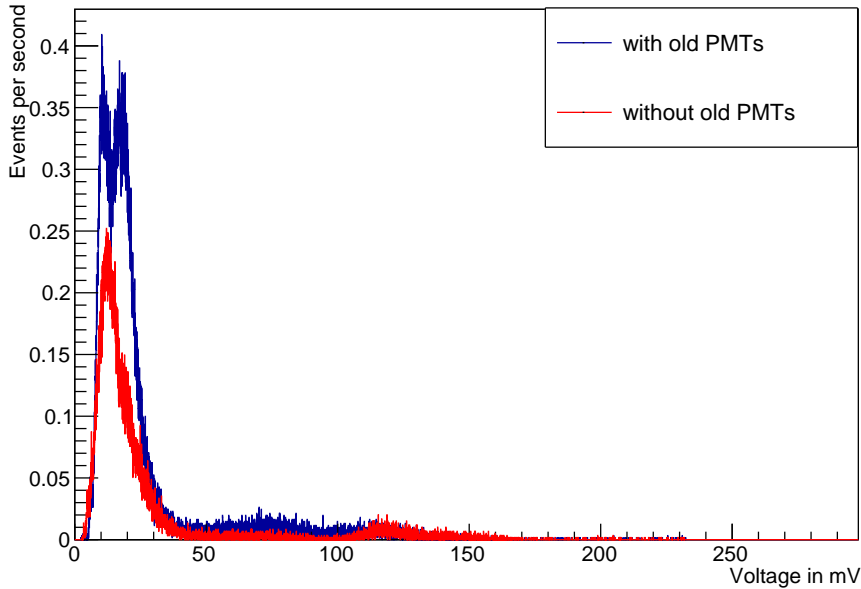
Figure 16: This show the improvement of the dark current after the old PMTs were taken out. The red line shows the spektrum after the PMTs were taken out and the blue shows it before.

the later peaks are insignificant compared to them. They all show two significant peaks, the first around $7\,\mathrm{mV}$ and the second one around $12\,\mathrm{mV}$. As the second peak corresponds to the same channels as LED pulses 18, it is indicated that there is still a bit of light in the box, which is observed from the PMT. The first peak is caused by thermionic dark current. As thermionic electrons are not multiplied as much as photoelectrons, they are found in lower voltage regions of the spectrum than the signals caused by light. Because the threshold is still cutting off signals even though it was set on 0, the peak structure becomes sharper. It becomes obvious that the higher the supplied voltage the higher the number of received signals, as this can be seen in all channels except for a supply voltage of $2000\,\mathrm{V}$ with signals between 30 and $40\,\mathrm{mV}$. Also all signal shift to higher voltages with a higher supply voltage applied, because the electric field accelerating the electrons inside the PMT is getting stronger. Thus the electrons will be multiplied more often. After the first two peaks a valley at circa $30\,\mathrm{mV}$ is observed. For the voltages above $1800\,\mathrm{V}$ the valley is followed by a peak. This peak is likely the characteristic second peak from photon related signals as we see in figure 18. The spectres with a supply voltage higher than $2000\,\mathrm{V}$ show a peak a $80\,\mathrm{mV}$. This leads to believe that this is a signal resulting from after pulses, as the electrons need to have a specific energy to ionize the gas clouds. Also
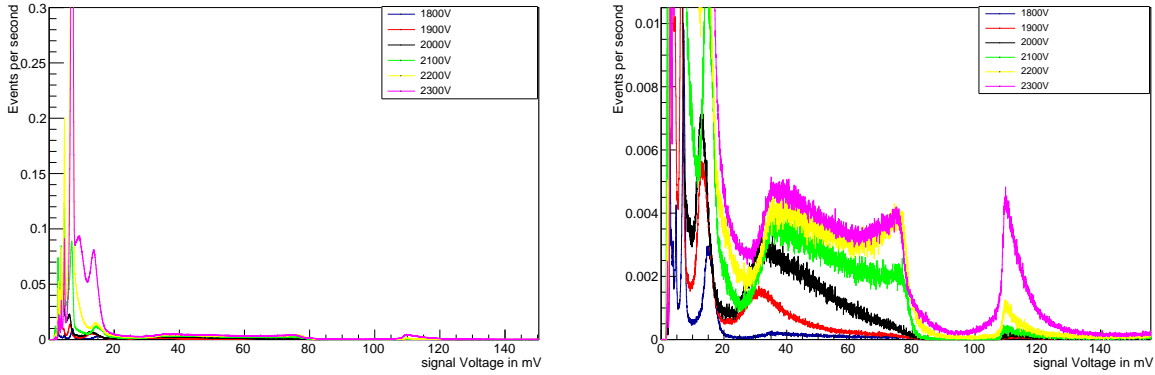
Figure 17: Dark current spectrum in dependency on the supply voltage. This shows the number of events per second for each channel. The channel numbers have been translated to the PMTs output signal voltage in mV using equation(26) and figure 14. The blue spectrum is the spectrum taken with a supply voltage of 1800 V, red shows 1900 V, black 2000 V, green 2100 V, yellow 2200 V and pink represents 2300 V.

the signal voltage is so high in comparison with the later measured single photon peak, that it is most likely caused by an after pulse or radio emission from the glass. This is, because other effects would require to release at least 6 photons at the same time from the photocathode. Because of the large difference between the spectrum from 2300 V and the rest at a signal voltage of 110 mV, this peak can only be a result of after pulses or an effect caused by the radiation of the environment with a drastic change at the time this spectrum was taken. But as the spectrum of 2200 V shows a similar form and as it has a big difference to the previous ones, the first possibility is far more likely. Also the measurement of 1800 V was taken between these two measurements, which shows that it cannot be caused by the same background signal, as it would have influenced this measurement too.

To classify the dark current the spektrum of the LED was taken at first with the oscilloscope and then with the ADC, which can be seen in figure 18. For the ADC the voltage of the LED was increased in 0.01 V steps from 1.18 V to 1.24 V. The PMT had a supply voltage of 2450 V during these measurements. The dark current was plotted in light blue to have a direct comparison of the spectres. In the plots with the LED we see two peaks with the second on loosing relevance for higher voltages. This is expected as the second peak is clearly visible in single photon event, but losses relevance the higher the photon number in an event. In the measurements we see that the first peak from the smaller voltages is a bit before the second peak from the dark current. But the first peak from 1.22 V is directly over it, which leads to believe that the second peak from the

40

dark current is caused by multi photon events. Also both peaks shift to the right as the voltage of the LED increases, as the number of photons the LED measures rises. Because the second peak of 1.22 V is also at the same intensity as the peak directly after the light peak in 17, it is believed that there is really an unidentified light source influencing the measurements. And that both peaks are caused by a multi photon events, corresponding to an LED with a voltage of 1.22 V. As the first peak with the lowest voltage is around
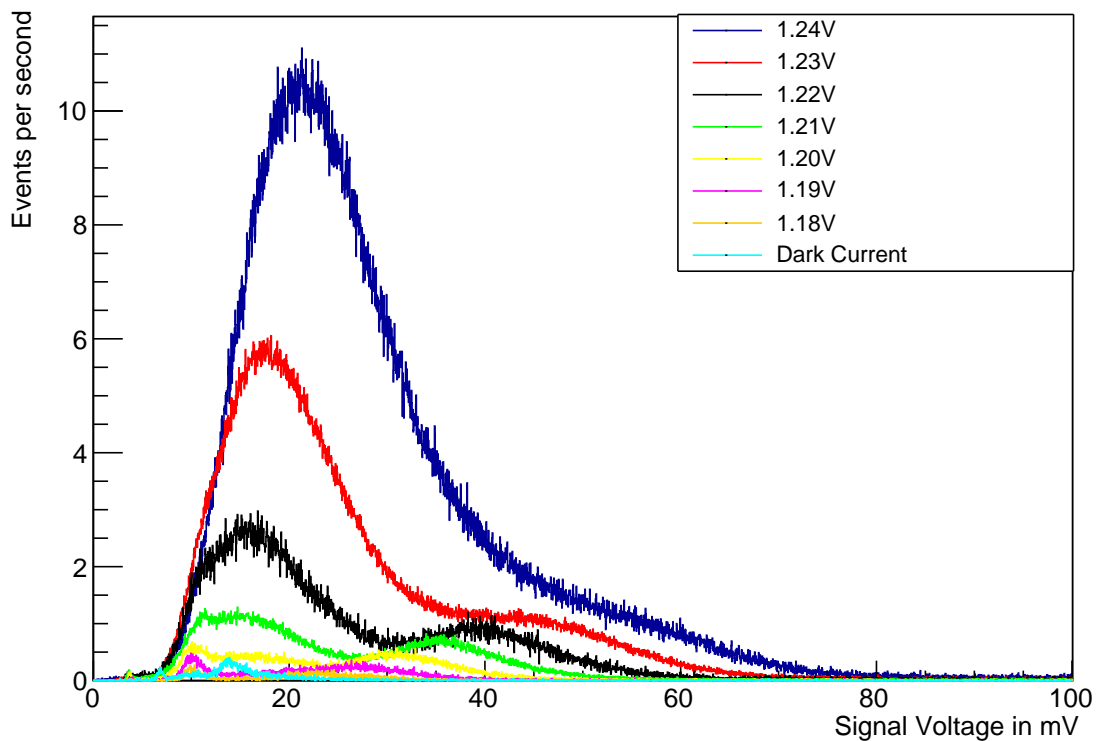
Figure 18: Measurements with just an LED in front of the PMT.

12 mV it was suspected that these could be caused by single photon events. To test it a 12 mV pulse from the LED was recorded with the oscilloscope. This is done by placing the LED with a voltage of 1.19 V in front of the PMT. The measurement can be seen in 19. With the pulse form and the resistance, which is typically around 50 Ω, the gain can be calculated using:

$$\delta = \frac{1}{eR} * \int u(t)\, dt. \tag{27}$$

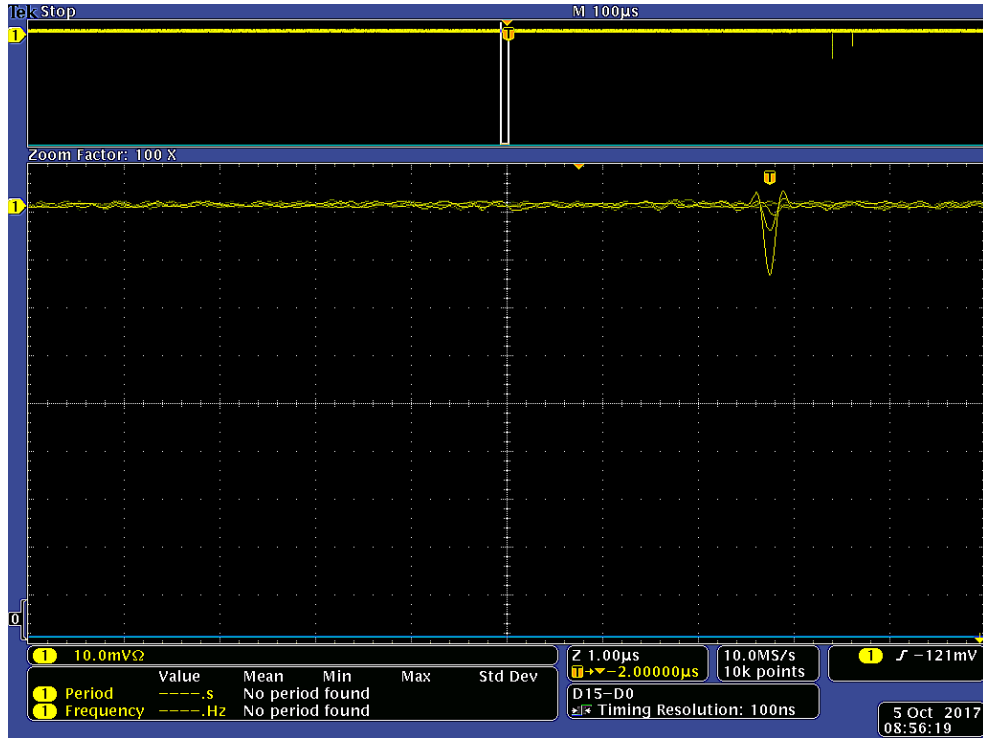With e being the elementary charge, δ the gain, R the resistance and $u(t)$ the voltage in

Figure 19: Measurement of a 12 mV light pulse fom the LED with the oscilloscope

dependency on the time. As the pulse from the measurement in 19has a width of around 250 ns, the gain results to $\delta = (1.87 \pm 0.39) * 10^7$. This is done by approximating the pulse with an isosceles triangle. The uncertainty is mostly influenced by the time resolution of the oscilloscope, which is only 100 ns. The bad time resolution is also the reason, why no better approximation was taken. The measured gain indicates that this should be an single photon event or at least an event in the same voltage region, as the manufacturer's data say that the gain should be $2 * 10^7$[45], which is within the deviation of the measurements. The gain the company states is higher than the measured gain, because the approximation with an isosceles triangle is not that accurate and the triangle is not as wide at the top as the pulse. Therefore the measured gain is expected to be slightly smaller than the real one.

3.3.3 Glue Measurements

In the PMT testing facility in China the 20-inch PMTs were tested in front of tubes. The inside of these tubes was covered with Tyvek foil to ensure a homogeneous distribution of the light from the LED. Because the dark current rate with the tubes in front of the PMTs was higher by 5 kHz than without the tubes, the Tyvek foil and the glue were measured. For this the same circuit as in chapter 3.3.2 was used, but a piece of cardboard with glue on or the Tyvek foil directly was placed in front of the PMT. These measurements were directly followed by the measurement of the dark current as in chapter 3.3.2. All measurements in this chapter will be conducted with a supply voltage of 2450 V. The measurements did not show the expected increase in the dark current rate, but rather a decrease. This can be seen in figure 20. As the decrease happens just before the second peak, which corresponds to light, the cardboard or the glue had to block light from getting to the PMT. All glues showed a similar spectrum. For figure 20 the UHU glue was picked, because the effect was the strongest there. The spectres of the other glues are in the appendix A. Because the glue
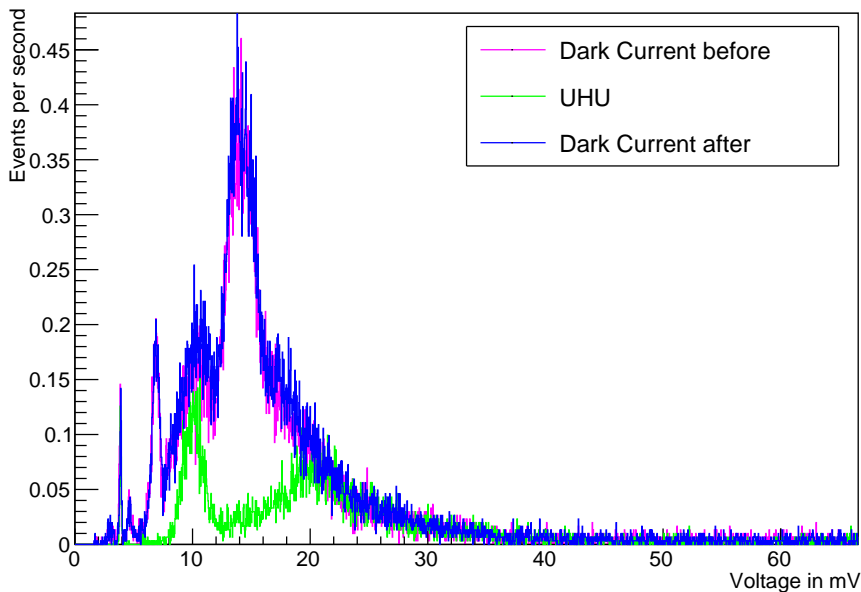

Figure 20: The red line shows the dark current before the measurement. The green line shows the spectrum with glue on cardboard in front of the PMT. The blue line shows the dark current spectrum after the measurement. The glue used for this picture is UHU.

was put in front of a cardboard, it was suspected that the cardboard blocked light. This was tested by only putting a piece of cardboard in front of the PMT. But the spectrum

of this measurement was equal to the dark current spectrum taken before and after the measurement as seen in figure 21.
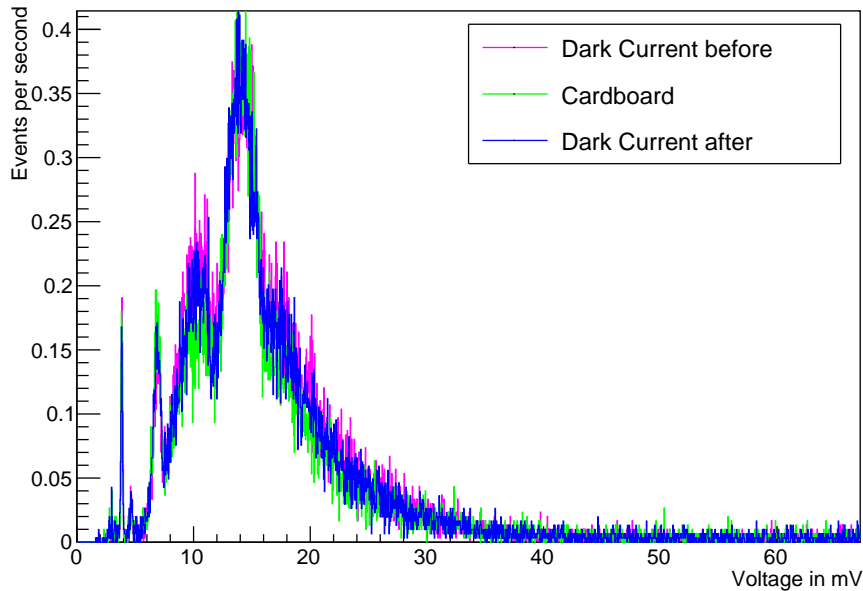

Figure 21: This measurement was taken with just cardbaord in front of the PMT. The grenn line shows the spectrum of the card board and the other the dark current spectrum.

So the effect, observed in China, had to be caused by the transportation, the time the tubes were stored or a chemical reaction with a substance that is more frequent in the different environment. As old glue tends to get weaker and the Tyvek is slowly released, the Tyvek foil was ripped off the cardboard to simulate just this. These measurements resulted in an increase of at least 18 Hz as seen in table 2 and figure 22. To compare it with figure 20 the glue used for figure 22 is UHU as well. The spectres of the other glues are also placed in the appendix A. This shows that the increase is happening at the same point in respect to the dark current peaks as the decrease in figure 20. The increase and decrease do not happen at the same Voltages, because the whole spectrum moves apart. This may have happened, because the errors of the ADC, which developed over time, grew stronger or because the supply voltage was changed accidentally. The expected increase of the dark current by scaling back the 5 kHz signal for a PMT that has a hundredths of the area would be 50 Hz. This was also measured with the Lyreco. This leads to believe that this is the same effect. An explanation for this effect would be that the excitation energy shifts according to the Stark effect. This is caused by the dipolmoment changing the
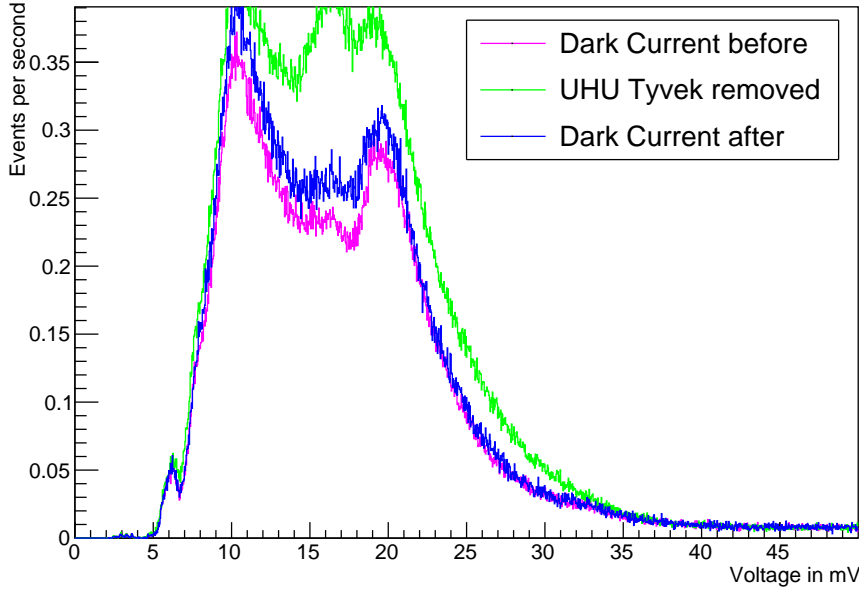
Figure 22: This shows a comparison of the spectrum of glue with Tyvek ripped off and the dark current spectrum. The green spectrum is the spectrum with cardboard and glue, where the tyvek foil was ripped off. The magenta coloured spectrum is the dark current before the measurement and the blue one corresponds to the dark current after the measurement.

Table 2: Measurements of glue after the Tyvek foil was pulled down half way

Glue	darkcurrent rate before in Hz	rate with glue in Hz	darkcurrent after in Hz
UHU	146.45 ± 1.16	175.01± 1.38	150.58± 1.2
Tape	150.58±1.2	194.65 ± 1.52	150.33 ± 1.22
Weicon	150.33 ± 1.22	170.85 ± 1.34	152.79 ± 1.23
Lyreco	152.79 ± 1.23	222.12 ± 1.69	176.29 ± 1.4

potential and localization uncertainty of the electron, which is responsible for the hydrogen bonding. Through these bindings glue can stick to other surfaces. The moment the dipole bonding is broken apart the excitation energy shifts back and the energy of the excited electron is released in form of a photon. While our measurements show a decrease of this effect over time, the effect in China will not show this until the Tyvek is not stuck to the tubes anymore. Because every single, tested glue shows this effect, the Tyvek foils cannot be stuck to the tubes using glue. Instead they will be applied to the tubes using staples. The staples are made out of stainless steel, because stainless steel is not magnetizable in most cases. If specially ordered stainless steel can be made magnetizable, by substituting carbon fibers with metal fiber. Thus the risk of magnetization is deemed negligible. The

only factor important for the measurements is the reflectivity of the staples. This could cause a decrease of signals in LED tests. But as the dark current is not influenced as seen in figure 23, this is not important for the testing. Also the area of the staples is so small that the decrease in reflection is irrelevant.
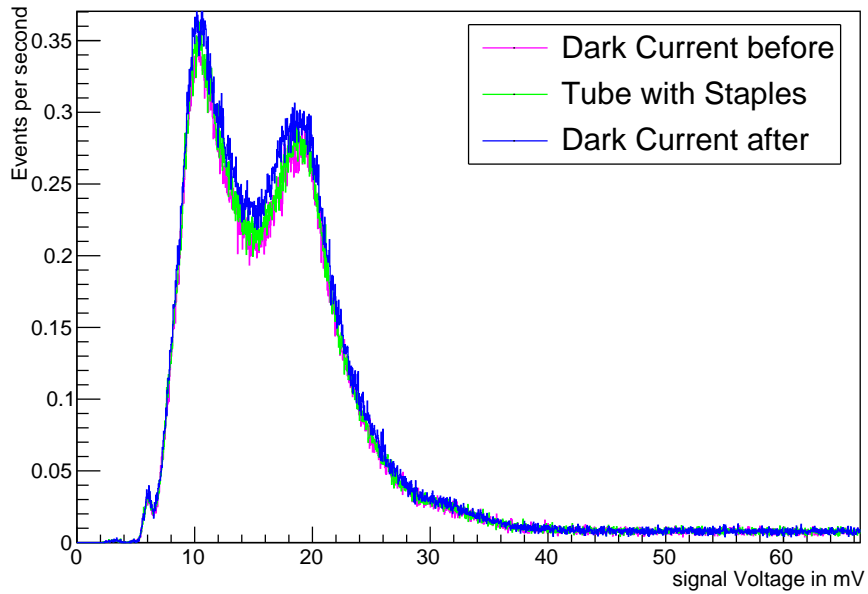

Figure 23: This picture shows a comparison between the pure dark current and the dark current with the PMT inside the tube.

3.3.4 Coincidence Measurements

For coincidence measurements an LED was placed in front of the PMT. To guarantee that the PMT is not damaged during this time, the LED is placed inside a 1.2 mm collimator. A diffuser was placed on the other end of the collimator to further reduce the light intensity.

A coincidence circuit can help to reduce background signals. The pulse generator sends 257 ns pulses to the LED and the amplifier from CAEN with a frequency of 1 kHz. The amplifier divides the signals in two. One of the outputs leads to a scaler to count how many pulses are sent. The other opens a 1 μs gate at the dual gate, which is send to the logic unit. The light of the LED is registered by the PMT and sent to the discriminator with the background signals. The discriminator cuts off all signals that are below the threshold. It is used to get rid of the thermionic dark current as they have a lower intensity. The signal from the discriminator is also send to the logic unit. Only when the gate and the discriminated signal from the PMT reach the logic unit at the same time a signal will be send to the amplifier from Ortec. From there the signal will be send to the scaler to count the number of coincidence events. The amplifiers are only used because the scaler could not detect the signals without it. The schematic overview of the circuit can be seen in figure 24. Here AMP stands for amplifier, HV is the high voltage supply unit, DG is the dual gate, Disc is the discriminator and AND is the logic unit. In this measurement
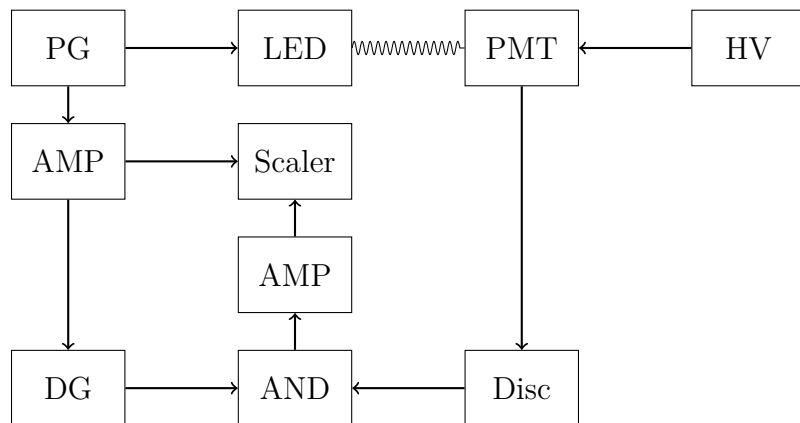

Figure 24: Schematic overview of the coincidence circuit

the PMT is operated with a constant voltage of 2450 V. It is assumed that the number of

photoelectrons is Poisson distributed. The mean value of photoelectrons is given by:

$$-\ln(1 - \frac{N_c}{N_P}) = pe. \tag{28}$$

Here pe is the number of photoelectrons, N_c is the number of coincidence signals and N_P is the number of LED pulses. As the stability of the pulse generator and the LED is unknown, the uncertainty of the measured number of events is estimated to Gaussian distributed. With a threshold of $9\,\mathrm{mV}$, the number of coindcidences and pulses was measured, while the intensity of the LED was increased by applying more voltage to the LED. This threshold was taken, because the single photon event corresponds to a voltage of $12\,\mathrm{mV}$, so these signals are not influenced by the threshold. The standard threshold of $\frac{1}{4}$ of the single photon event was not used as the discriminator created massive noise at this setting, which will be mentioned later. The voltages between 1.17 and $1.25\,\mathrm{V}$ were chosen, because the PMT begins to notice the LED's signals at $1.17\,\mathrm{V}$. The results of the measurement can be seen in table 3. This shows that the number of photoelectrons is dependent on the intensity

Table 3: Number of photoelectrons in dependency on the voltage of the LED. The threshold was set on $9\,\mathrm{mV}$.

Voltage in V	Number of Pulses	Number of Coincidences	Number of Photoelectrons
0	300925 ± 549	62 ± 8	$(2.06 \pm 0.26) * 10^{-4}$
1.17	320152 ± 569	1887 ± 43	$(5.91 \pm 0.14) * 10^{-3}$
1.18	323534 ± 566	3629 ± 60	$(1.13 \pm 0.02) * 10^{-2}$
1.19	321156 ± 549	7416 ± 86	$(2.34 \pm 0.03) * 10^{-2}$
1.2	301032 ± 550	14059 ± 119	$(4.78 \pm 0.04) * 10^{-2}$
1.21	303018 ± 549	26617 ± 163	$(9.19 \pm 0.06) * 10^{-2}$
1.22	300808 ± 549	44032 ± 210	0.158 ± 0.001
1.23	300806 ± 551	70836 ± 266	0.269 ± 0.001
1.24	304138 ± 549	105404 ± 324	0.426 ± 0.002
1.25	301362 ± 549	136377 ± 369	0.602 ± 0.003

of the LED. The number of photoelectrons without light is this high in comparison to the number of photoelectrons with light on, because the LED used in this measurement is not stabilized. A stabilized LED would always send out the light at the point of the pulse. A non stabilized LED sends the signals at varying times during the pulse. This causes the LED pulses to be Gaussian distributed around a certain time in the pulse width of the generators pulses. This measurement can later be compared with the stabilized LED that is screwed into the collimator.

After this measurement the threshold of the discriminator was tested with a constant voltage on the LED of 1.2 V. As the discriminator cuts off all signals below the adjusted voltage, it is expected that the number of coincidences per pulse decreases with an increase of the threshold. Additionally it is expected that the number of coincidences drastically decrease after 20 mV as the first peaks of the LED end there as seen in figure 18. That this is not the case can be seen in table 4. Between the threshold settings 4 and 6 the

Table 4: Number of photoelectron in dependency on the threshold. The LED was tested with a voltage of 1.2 V.

Threshold in mV	Number of Pulses	Number of Coincidences	Number of Photoelectrons in 10^{-2}
0	302486±550	11814 ±108	3.98±0.04
3	313132 ±560	156108±395	69.02±0.31
4	309470 ±556	154214±392	68.98 ± 0.31
6	302954 ±550	14593±120	4.94±0.04
9	301032±549	14059±118	4.78 ± 0.04
12	301566±549	13737±117	4.66±0.04
30	359462±599	15111±123	4.29±0.04
90	300838± 549	2912± 54	0.97 ±0.02

expected rapid decrease in rate can be seen, when a peak structure is cut off. After this a long phase were the rate only decreases slowly can be seen between the settings 6 and 12. A problem is that the number of measured signals with a threshold of 0 mV is about equal to the measurements with a threshold higher then 6 mV and therefore about ten times lower then the number of coincidences with a threshold of 3 and 4 mV. Also the first cut off is too early, while the second peak is not cut off after the expected voltage. Also the cut off effect from the dark current would be far to great to be caused by the cut off of thermionic dark current. This could be a result of background noise created by the discriminator at 3 and 4 mV. This was observed by only connecting the discriminator to the oscilloscope. When the threshold was set on 3 mV and 4 mV the oscilloscope showed that signals where transmitted. On the other settings the oscilloscope did not show any signals. This means that either the threshold is not working at all or that it just has a big off set. As the number of signals greatly decreases with a threshold of 90 mV as seen in 4, the second possibility is more likely. This was also verified using the oscilloscope. Because the laboratory does not have a reliable source for constant low voltage signals, the offset cannot be determined as of now.

4 Conclusion and Outlook

During this thesis the second out of four test facility for the characterization of 20-inch photomultiplier tubes (PMTs) was constructed and placed inside a shipping container. These containers have a passive shielding against the earth magnetic field to reduce the magnetic flux to 10%. The magnetic field inside this container and two other containers was measured and means to decrease the magnetic fields were taken. The measurements indicate that the magnetic field meets the requirements at most points. It was identified that the magnetic fields inside them grow stronger in course of the transportation. A quick way to strengthen the shielding was developed by covering the damaged parts at the door with a fine matt foil. With this most of the covered points that did not met the before, met the requirements afterwards. Also none of the covered points had a magnetic flux so high, that it would likely influence the measurements.

Inside the laboratory the small test stand was commissioned. The dark current rate was reduced by removing PMTs, which were not used for the measurements, from the test stand. For the characterization of the PMTs first the analog to digital converter's (ADC) errors were characterized. After this, dark current measurements were taken. These showed the expected behavior, when the supply voltage was increased. Most of the peaks in the spectrum have been characterized. The dark current spectres showed an unexpected behavior, which is probably caused by an external signal getting into the test facility. As it corresponds to the same voltage region of around $12\,\mathrm{mV}$, where the single photon peaks are expected, based on measurements with an LED.

Inside the containers the PMTs will be placed in front of the tubes. The inside of these tubes is covered with Tyvek foil. For the first container that already reached the testing site, the foil was applied to the tubes using glue. Because the dark current rate was greatly increased inside these tubes, the effect of glue and Tyvek on the dark current rate needed to be determined. Therefore the the glue, which connects the Tyvek and the tubes, and the Tyvek were examined by placing them in front of the small PMT. While Tyvek showed no effect on the dark current rate, the glue that was placed on cardboard showed a decrease of the rate. Also the combination of cardboard, Tyvek and glue showed this decrease. When the Tyvek was ripped off the cardboard an increase of the rate was observed at the same place inside the spectrum as the former decrease. This leads to believe that the glue's excitation energy that is minimally shifted by the dipole moments via the Stark effect.

This causes the glue to absorb light, while the dipole moments are intact. When the dipole moments are dissolved the excitation energy is shifted back. The excited electron then sends out a photon as it falls back on the ground state. This can be avoided by using staples instead of the glue to fixate the Tyvek on the tubes.

After this a coincidence circuit was constructed to reduce the background noise. As the LED was not stabilized the measurements are not as representative as they should be. In the future a stabilized LED can be used. Also either the threshold of the discriminator will be characterized or a new discriminator will be used to further improve the circuit.

Additionally the peak to valley ratio can be measured, now that the voltage region in the spectrum of the PMT, where single photon events of the PMT are expected, is known.

Also the transit time spread can be measured by using a ps-laser and a time to digital converter (TDC) or a combination of a time to amplitude converter (TDA) and an ADC, which creates a TDC.

Because ADCs cannot plot the forms of the pulses, it is planned to use a Flash-ADC in the future to increase the relevance of the measurements.
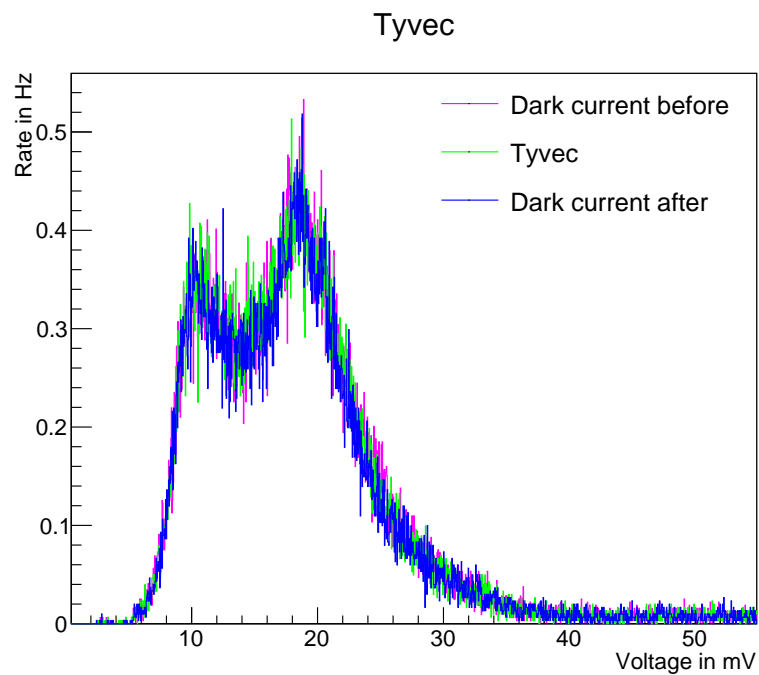
A Other Measured Glues

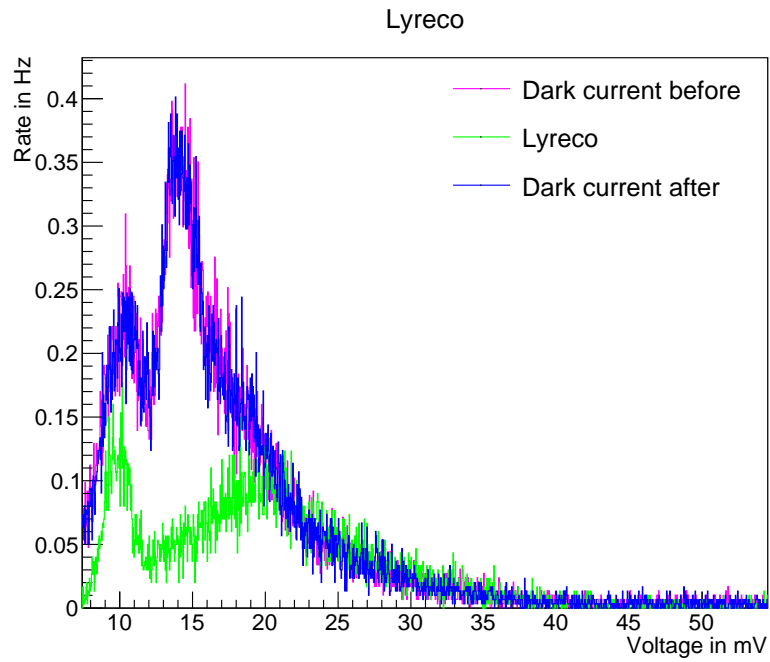Figure 25: Spectrum of just Tyvek foil in front of the PMT

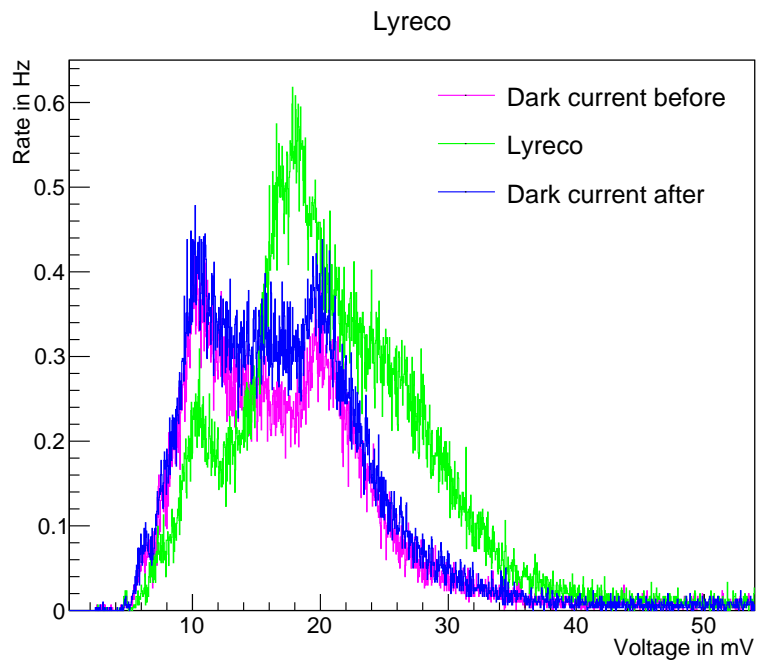Figure 26: Spectrum of cardboard with Lyreco glue in front of the PMT

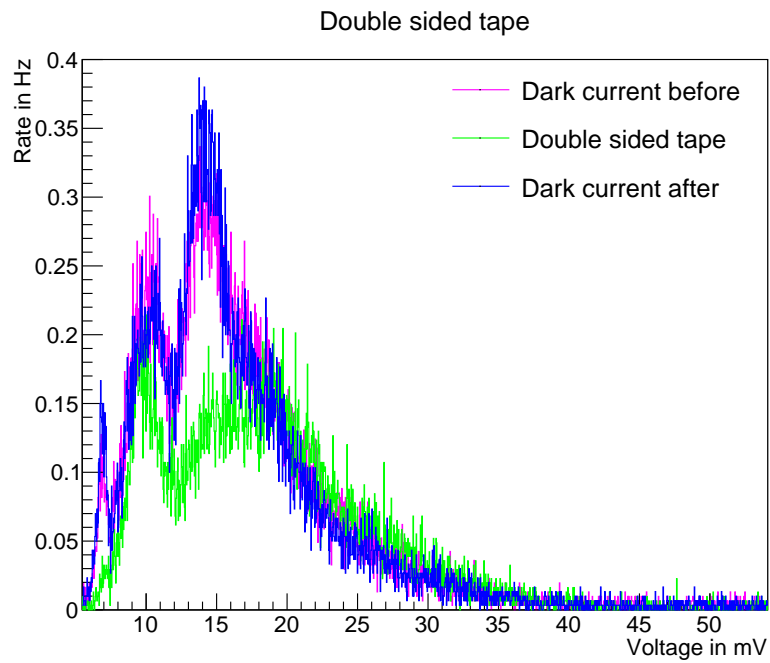Figure 27: Lyreco Glue with the tyvek foil ripped off

Figure 28: Spectrum of cardboard with double-sided tape in front of the PMT
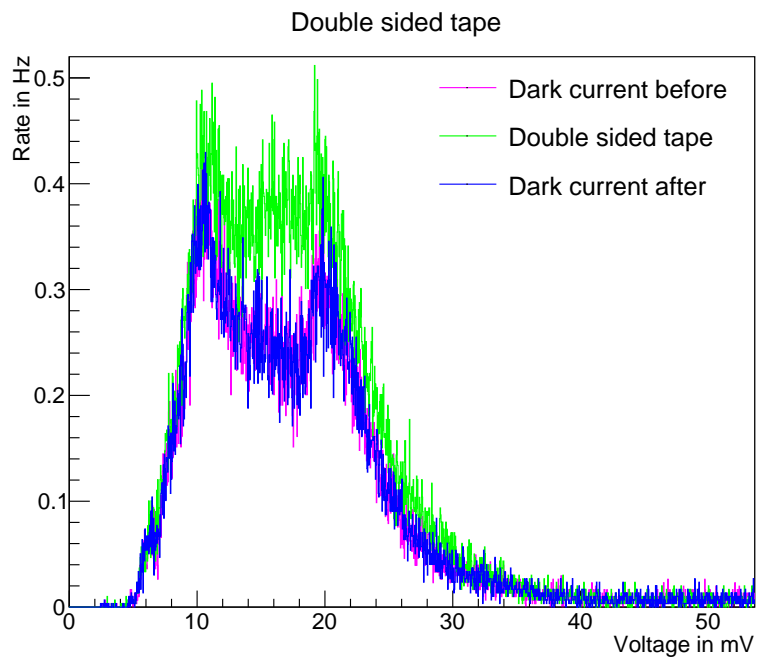

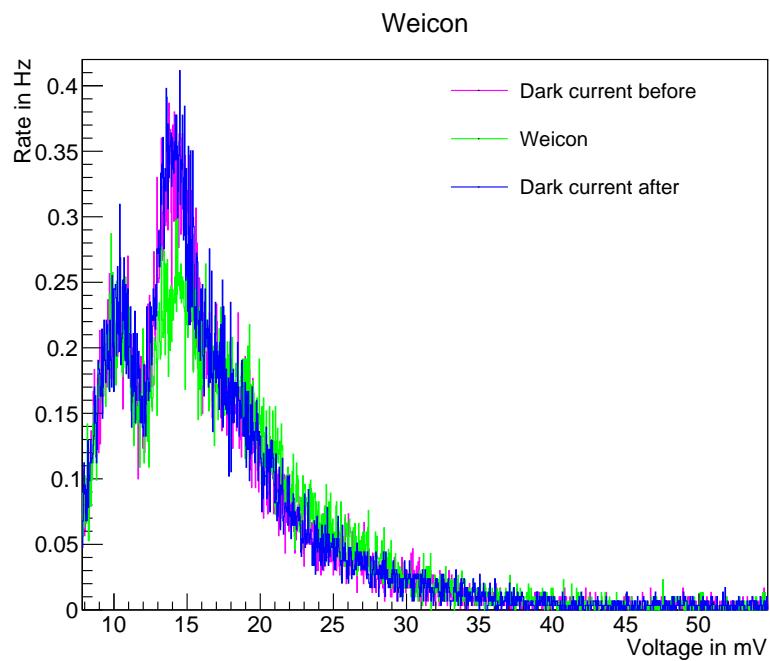Figure 29: double-sided tape with the tyvek foil ripped off

Figure 30: Spectrum of cardboard with weicon adhesive spray in front of the PMT
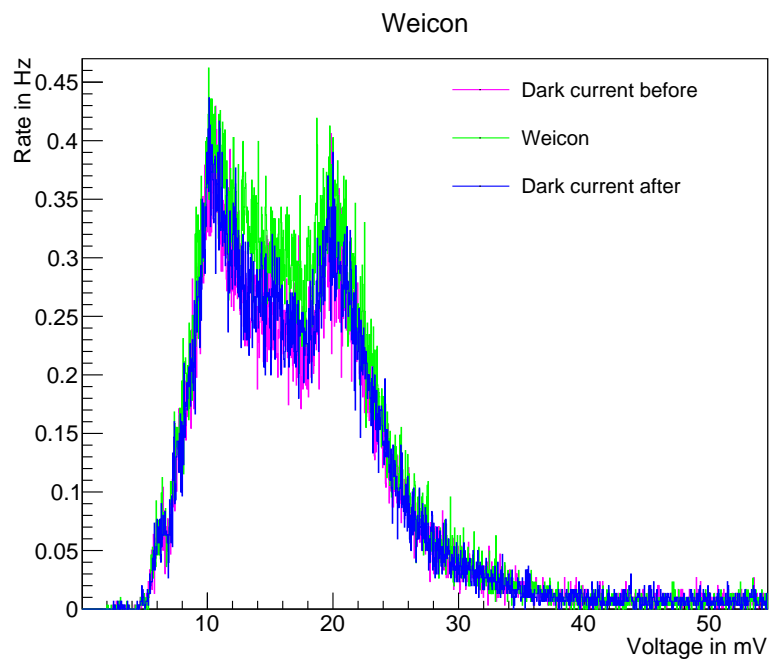

Figure 31: Weicon adhesive spray with the tyvek foil ripped off

References

[1] David Griffith *Introduction to Elementary Particles, 2008*

[2] Universität Zürich group Serra *http://www.physik.uzh.ch/groups/serra/StandardModel.htm*

[3] Patrignani C. et. al. *Review of Particle Physics*in *Chin. Phys.*,2016

[4] C.S. Wu et al. *Experimental Test of Parity Conservation in Beta Decay*in *Physical Review*,1957

[5] Goldhaber,L.Grodzins,and A.W.Sunyar.*Helicity of Neutrinos.*In *Physical Review*,1958

[6] Kai Zuber *Neutrino Physics 2 ed*, 2012

[7] Haoqui Lu *The Status of JUNO* in *Conference Talk*, 2016

[8] Felix Benckwitz, unpublished Bachelor thesis, 2017

[9] Thierry Lasserre and Henry W. Sobel *Reactor Neutrinos* in:*Comptes Rendus Physique*, 2005

[10] Universität Hamburg Forschungsgruppe Neutrinophysik
http://www.neutrino.uni-hamburg.de/projekte/juno/

[11] Liang Zhan *talk:Flavour Physics Conference*, 2017

[12] HAMAMATSU PHOTONICS K. K. *PHOTOMULTIPLIER TUBES: Basics and Applications, 2007*

[13] Benedict Kaiser *Commissioning of a test facility to charaterise JUNO photomultipliers*, Bachelor thesis, Hamburg, Germany: Universität Hamburg, 2016

[14] Fengpen An et al. *Neutrino Physicsd with JUNO* in *Journal of Physics G: Nuclear and Particle Physics* 2015

[15] F.Capozzi et al. *Status of three neutrino oscillation parameters, circa 2013*in*Physical review D 89.9*,2014

[16] Luca Stanco et al. *A new way to determine the neutrino mass hierarchy at reactors* arXiv:1707.07651, 2017

[17] Hans-Thomas Janka *Neutrino Emission from Supernovae* arXiv:1702.08713 ,2017

[18] Yoichiro Suzuka *Solar Neutrinos*, 1999 *http://www.slac.stanford.edu/econf/C990809/docs/suzuki.pdf* (visited on 5.9.2017)

[19] N.Anfimov *Large photocathode 20-inch PMT testing methods for the JUNO experiment* in*Journal of instrumentation*, 2017

[20] Kaijie Li et al. *Poster for LP17*

[21] CAEN *N957 user manual Revision no.8*, 2017 *http://www.caen.it/csite/CaenProd.jsp?idmod=466&parent=12*

[22] L.Ludhova and S.Zavatarelli *Studying the Earth with Geoneutrinos*arXiv:1310.3961v2, 2017

[23] Stefan Mayer Instruments *Magnetfeldsensor FLC3-70: Dreiachsiger Fluxgate-Sensor für schwache Magnetfelder*

[24] Agilent Technologies *Agilent 81100 Family of Pulse Pattern Generators* Data sheet version1.3 *http://literature.cdn.keysight.com/litweb/pdf/5980-1215E.pdf?id=1000068892:epsg:dow*

[25] Advanced Measurement Technology, Inc. *Ortec Part No. 733370 Manual Revision D*

[26] Sebastian Lorentz *Topological Track Reconstruction in Liquid Scintillator and LENA as a Far-Detector in an LBNO Experiment* Dissertation, 2016

[27] Lisa Steppat *Development and commissioning of the setup for masstesting of JUNO PMTs* Master thesis, 2017

[28] Joseph R. Icadela et al. *Status and Prospects of Top-Quark Physics*in *Prog.Part.Nucl.Phys.*,2009

[29] Miao He *Jiangmen Underground Neutrino Observatory*, 2014

[30] B.Pontecorvo,*Neutrino Expeiments And The Problem Of Conservation Of Leptonic Charge*, in *Soviet Physics JetP*,1968

[31] G.Danby et al., *Observation of High-Energy Neutrino Reactions And The Existence Of Two Kinds Of Neutrinos*, in *Phys. Rev. Lett. 9*, 1962

[32] Chris Polly.*Neutrino History 1927-1987:1930 Pauli neutrino letter(translated by Kurt Riesselmann*
URL:http://microboone-docdb.fnal.gov/cgi-bin/
RetrieveFile?docid=953&filename=pauli%20letter1930.pdf&version (visited on 30.08.2017)

[33] C.Regis et al. *Search for Proton Decay via $p \rightarrow \mu + K^0$ in Super-Kamiokande I, II, and III* arXiv:1205.6538v1, 2012

[34] SNO Collaboration, ed. *Measurement of charged current interactions produced by B solar neutrinos at the Sudbury Neutrino Observatory*,2001

[35] O.Smirnov *Status of PMT geomagne0c field shielding*, talk for *JUNO10 Collaboration Meeting* , 2017

[36] James W. Corwin *CP SYMMETRY VIOLATION - THE SEARCH FOR ITS ORIGIN* in *Nobel lecture 8*, 1980

[37] Et-Enterprises *determination of the multiplier gain of a photomultiplier*, 2011
http://www.et-enterprises.com/files/file/technical-information/rp076_determination
%20of%20multiplier%20gain%20of%20pmt.pdf

[38] HAMAMATSU PHOTONICS K.K *R1828-01 Datasheet*, 2000

[39] CAEN *Mod. N844/N844P/N845* in *Technical Information Manuel revision no.7*, 7.2011

[40] CAEN *Mod. N978* in *Technical Information Manual revision no.5*, 2.2011

[41] CAEN *Mod. N455* in *Technical Information Manual revision no.2*, 10.2004

[42] HAMAMATSU Photonics K.K. *Photomultiplier Tubes Recent Trend of PMTs URL: http://www.lns.tohoku.ac.jp/workshop/c010/slides/011.pdf for HEP & Scintillation Application*, 2015

[43] Takuya Yonekura et al. *Performance of the MCP-PMTs for top counter in Belle II Experiment*, 2014

[44] Quingmin Zhang *JUNO Central Detector and its Calibration System* Poster for 38th *International Conference on High Energy Physics*, 2016

[45] HAMAMATSU Photonics K.K. *Photomultiplier Tubes R1828-01, R2059*,2010

[46] Shin-Shan Yu *Search for Higgs at CDF*, 2006

[47] L.Wolfenstein *Neutrino Oscillations in Matter*, 1978

[48] M.G. Aartsen et al. *PINGU: A Vision for Neutrino and Particle Physics at the South Pole*, 2017

[49] G.L. Fogli et al. *Combined analysis of KamLAND and Borexino neutrino signals from Th and U decays in the Earth's interior*, 2010

[50] Sen Quian and Shulin Liu *The 20 inch MCP-PMT R&D in China*, talk for 38th INternational Conference on High Energy Physics, 2016

[51] Horst Kuchling *Taschenbuch der Physik: Mit zahlreichen Tabellen*, 1995

[52] David Jiles *Introduction to magnetism and magnetic materials* 2 ed.,1998

[53] Shi-Jun Liang and L.K. Ang *Electron Thermionic Emission from Graphene and Thermionic Energy Converter*, 2015

Acknowledgements

First of all I would like to thank

Prof.Dr.Caren Hagner

for providing me with a place inside the neutrino physics research group to write my Bachelor thesis. Furthermore I would like to express my gratitude towards

Dr.Björn Wonsak

for letting me work inside the JUNO group, proofreading my thesis and the advice we got from him every time. I would like to give special thanks to

Malte Stender

for always helping me. Furthermore he wrote several programs used for analyzing the data and being a good coworker. Additionally he helped me improve my thesis by spell checking. The next person I would like to express my gratitude towards is

Henning Rebber

for proofreading my Bachelor thesis. Also special thanks to

Dr.Daniel Bick

for helping with hardware and software related problems and

Hans-Jürgen Ohnmacht

for helping me inside the laboratory by answering all hardware related questions I had. For all the fun we had during and outside the working time I would like to express my gratitude towards all the previously mentioned people and thew remaining part of the group

Felix Benckwitz, Stefan Bieschke, Dr.Joachim Ebert, Benedict Kaiser, Petra Hinzer, David Meyhöfer and *Dr.Björn Opitz.*

At last I want want to thank

Irina Chelysheva and my family: *Nicole Sorgenfrei, Heino Sorgenfrei, Michèle Sorgenfrei* and *Jasper Sorgenfrei*

for all the emotional support.

Eidesstattliche Erklärung

Hiermit erkläre ich an Eides Statt, dass die vorliegende Arbeit von mir selbständig verfasst wurde und ich keine anderen als die angegebenen Hilfsmittel, insbesondere keine im Quellenverzeichnis nicht benannten Internet-Quellen, benutzt habe. Sämtliche Stellen der Arbeit, die im Wortlaut oder dem Sinn nach anderen gedruckten oder im Internet verfügbaren Werken entnommen sind, habe ich durch genaue Quellenangaben kenntlich gemacht. Die Arbeit wurde von mir vorher nicht in einem anderen Prüfungsverfahren eingereicht. Die eingereichte schriftliche Fassung entspricht der auf dem elektronischen Speichermedium. Ich bin damit einverstanden, dass die Bachelorarbeit veröffentlicht wird.

Ort, Datum   Unterschrift

Statutory declaration

I hereby declare that I have authored this thesis independently and that I have not used other than the declared resources, in particular no Internet resources that are not labelled in the bibliography. I have explicitly marked all material which has been quoted either literally or by content from the used sources. This thesis has not been submitted in another examination procedure before. The submitted, written version conforms with the one on the electronic storage medium. I agree that the thesis will be published.

Location, Date   Signature